

Zeolitic Imidazolate Frameworks: Synthesis, Functionalization, and Catalytic/Adsorption Applications

Samiran Bhattacharjee · Min-Seok Jang ·
Hee-Jin Kwon · Wha-Seung Ahn

Published online: 20 August 2014
© Springer Science+Business Media New York 2014

Abstract Zeolitic imidazolate frameworks (ZIFs) are comprised of transition metal ions (Zn, Co) and a range of imidazolate linkers in a tetrahedral coordination similar to that in crystalline aluminosilicate zeolites. The high surface area, tunable nanoporosity that can be subject to functionalization and the excellent thermal/chemical stability of ZIFs are attractive for heterogeneous catalysis and selective gas adsorption/separation. This review presents the current trends in synthesis, surface modification and catalytic reactions/adsorption of ZIF-based materials with particular emphasis on ZIF-8, which is the most widely studied structure among ZIFs.

Keywords Zeolitic imidazolate frameworks (ZIFs) · ZIF-8 · Synthesis · Functionalization · Heterogeneous catalysis · Adsorption

1 Introduction

Zeolitic imidazolate frameworks (ZIFs) are a subfamily of metal organic frameworks (MOFs), and are composed of transition metals, such as Zn or Co atoms, connected to different organic imidazolate linkers in a tetrahedral arrangement. Systematic variations of the linker substituents have yielded a range of structures with similar topologies to those found in zeolites [1–4]. ZIFs have attracted considerable interest in recent years because of their potential applications in adsorption/separation [2–11] and

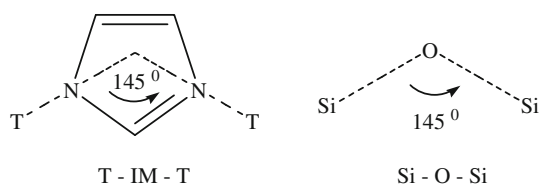
as a heterogeneous catalyst for a range of organic transformations [12–17].

The primary building unit of ZIFs is made of T–IM–T (T = tetrahedrally coordinated metal ion, IM = imidazolate and its derivative) bonding with a T–IM–T angle of 145°, which is similar to the Si–O–Si angle in zeolites (Scheme 1). The structure adopted by a given ZIF depends primarily on the type of imidazolate and solvent used, and greater structural diversity in ZIFs is possible using functionalized imidazolate ligands in their synthesis [3]. ZIF materials can have structures analogous to standard zeolite with a topology, such as *sod*, *rho*, *gme*, *lta*, and *ana*, employing a different imidazolate ligand, as shown in Scheme 2, as well as those previously unknown in zeolites using a mixture of two different imidazolate ligands. By implementing high-throughput synthesis technique, a large number of new ZIF structures was isolated [2] and approximately 105 ZIF materials with different chemical compositions or structures were reported by 2010 [4].

Most ZIFs are crystalline microporous materials with uniform micropores and a large cavity connected by small windows, and normally exhibit high thermal and chemical stability, as confirmed by thermogravimetric analysis (TGA) or by examining the X-ray diffraction (XRD) pattern of the material after a boiling test in water, methanol aqueous sodium hydroxide and benzene [1]. The crystal structure of ZIF-8, for example, was found maintained after suspending it in boiling water for 7 days.

Despite the structural diversity of ZIFs, ZIF-8 has been investigated predominantly for catalysis and adsorption because of its easy and reproducible synthesis. ZIF-8 has a *sod* topology that is formed by four- and six-member ring ZnN_4 clusters with internal cavities, 1.16 nm in diameter, connected by 0.34 nm windows [1]. ZIF-8 can also be obtained commercially as Basolite Z1200 from Aldrich.

S. Bhattacharjee · M.-S. Jang · H.-J. Kwon · W.-S. Ahn (✉)
Department of Chemistry and Chemical Engineering,
Inha University, Incheon 402-751, South Korea
e-mail: whasahn@inha.ac.kr



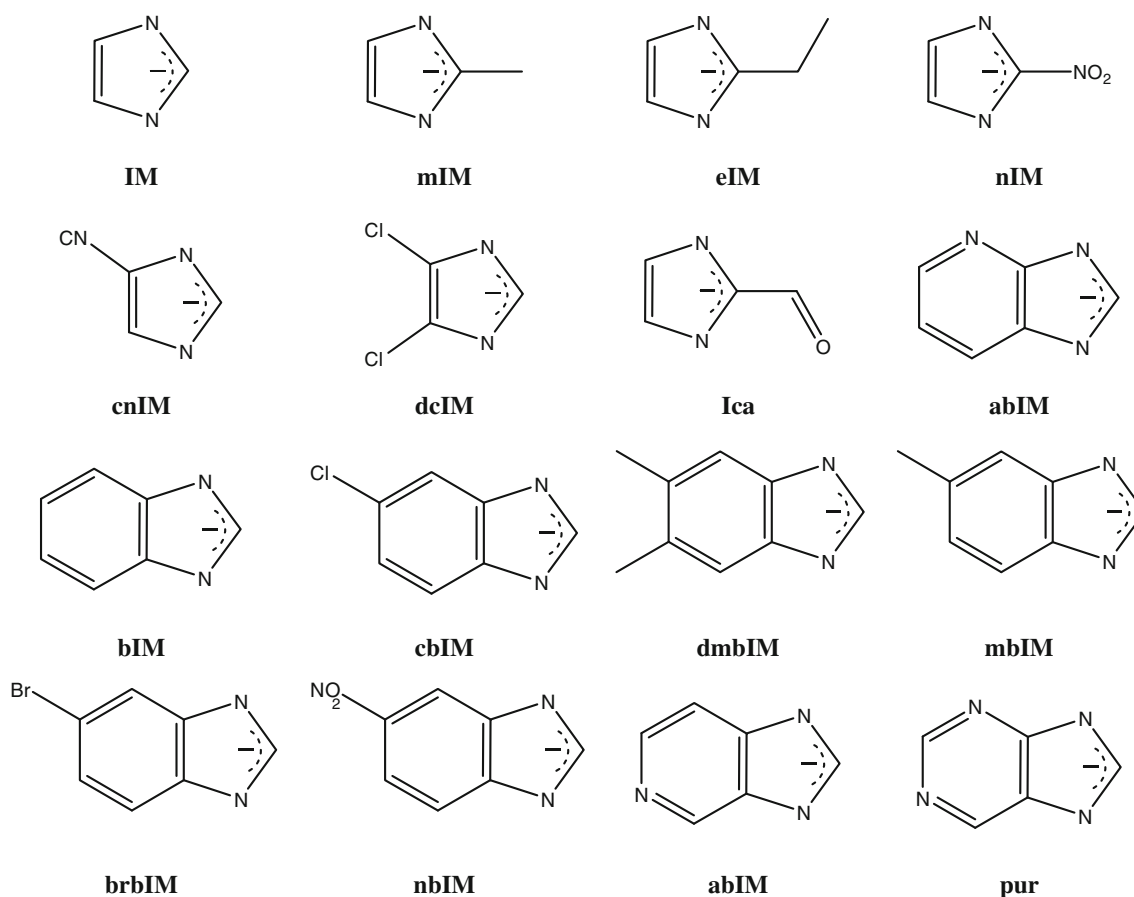
Scheme 1 Metal-imidazolite in ZIFs vs. Si-O bond angle in zeolites [1]

A limited number of other ZIF structures have also been considered for shape- and size-selective separations or for catalysis. Figure 1 and Table 1 present these representative ZIFs materials for catalysis and adsorption. Remarkably, fine-tuning of the pore size (from 7.1 to 15.9 Å) and surface area (620–1,730 m²/g) in ZIF with a *gme* structure was accomplished by conducting its synthesis using an equimolar mixture of 2-nitroimidazole (nIM in Scheme 2) and other imidazolates, as described in Fig. 2 [4]. The *gme* topology is the only one found in ZIFs with both large pores and large windows [5].

Yaghi and coauthors [3] also reported the synthesis of two mesoporous zeolitic imidazolite frameworks, ZIF-95

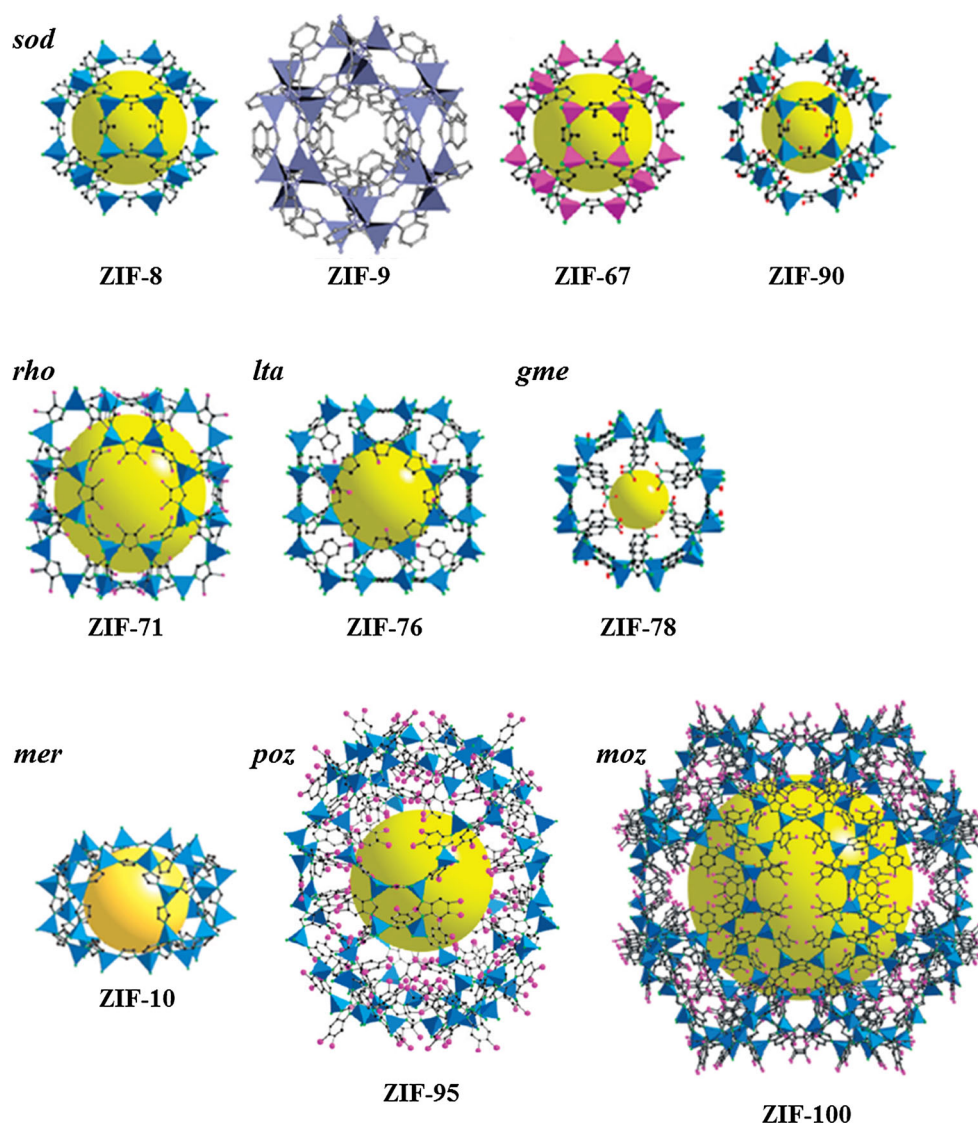
and ZIF-100. The frameworks of ZIF-95 are constructed from all tetrahedral Zn atoms linked through N atoms of 5-chlorobenzimidazole to form a neutral framework with two types of cages (smaller cage diameter 25.1 × 14.3 Å and larger cage diameter 30.1 × 20.0 Å), whereas ZIF-100 showed a complex structure, where one Zn atom was only tri-coordinated by imidazolite linkers with an outer and inner diameter of 67.2 and 35.6 Å, respectively.

Several extensive review articles dealing with the synthesis, structural description, functionalization, and adsorption/catalytic application of MOFs have been published [18–27], including one focusing specifically on CuBTC (BTC = benzene-1,3,5-tricarboxylate) to provide more engineering-orientated information on MOFs synthesis and their use as adsorption/catalysts in industry [28]. Regarding ZIFs, a short review on the synthesis of ZIF membranes/films and their application in gas and liquid separation and in functional devices have been reported [29]. This paper presents a report on the recent progress made on the synthesis, functionalization, and catalytic/adsorption studies concerning ZIFs.



Scheme 2 Imidazolite ligands used for ZIFs synthesis [4]

Fig. 1 Representative ZIF structures studied for catalysis/adsorption [1, 102]



2 ZIF Synthesis

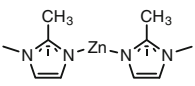
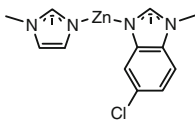
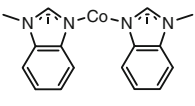
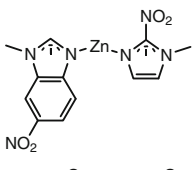
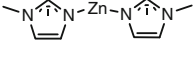
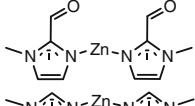
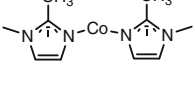
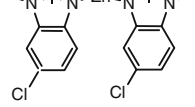
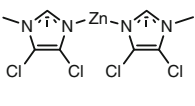
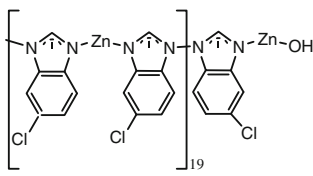
Most ZIF structures are prepared mainly by solvothermal/hydrothermal synthesis [1, 2, 30–38]. ZIFs can also be prepared by alternative synthesis methods, as listed in Table 2 for ZIF-8, such as microwave [7, 39–41], sonochemical [16, 42], mechanochemical [43–47], dry-gel conversion [48], solvent-free oxide/hydroxide-based [49, 50], microfluidic [51, 52], and electrochemical methods [53]. Figure 3 briefly summarizes the synthesis schemes employed [54].

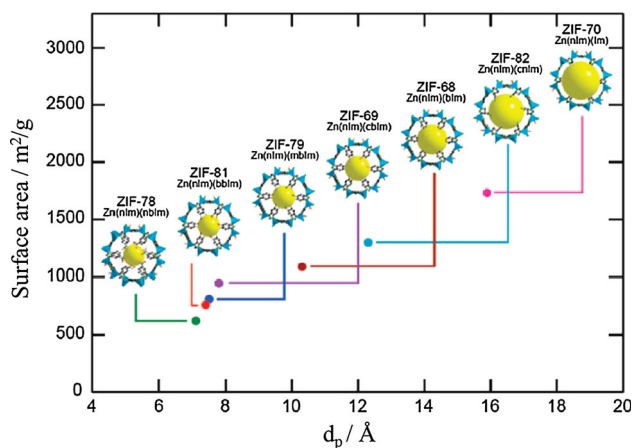
2.1 Solvothermal/Hydrothermal

ZIFs in general can be prepared by a solvothermal treatment at a substrate concentration of 0.2 M, a reaction time of 72 h, and isothermal temperatures of 358–423 K [2]. ZIF-8 is typically synthesized solvothermally using zinc

nitrate tetrahydrate ($\text{Zn}(\text{NO}_3)_2 \cdot 4\text{H}_2\text{O}$, 0.803 mmol) and 2-methylimidazole (HMeIM, 0.731 mmol) dissolved in *N,N*-dimethylformamide (DMF, 18 mL). The solution mixture was placed in a convection oven and heated to 413 K for 24 h [1]. After separating the mother liquor from the mixture, the solid crystals obtained were placed in 20 mL of chloroform, and the colorless polyhedral crystal product was collected. Finally, the product was washed several times with 10 mL of DMF, and dried in air. Nune et al. [30] reported the synthesis of ZIF-8 using methanol and 1 % high molecular weight poly(diallyldimethylammonium) chloride at room temperature to produce nanoparticles with a mean diameter of 57 ± 7 nm with a thickness of 42 nm measured by transmission electron microscopy (TEM) and electron tomography; poly (diallyldimethylammonium) chloride played a key role in controlling the morphology of nanoparticles. Pan et al. [31] synthesized ZIF-8 in an aqueous medium from a reaction

Table 1 Representative ZIF structures for catalysis and adsorption [4]

ZIF-n	Composition	Net code	Composition structure	ZIF-n	Composition	Net code	Composition structure
ZIF-8	Zn(MeIM) ₂	<i>sod</i>		ZIF-76	Zn(IM)(cbIM)	<i>lta</i>	
ZIF-9	Co(bIM) ₂	<i>sod</i>		ZIF-78	Zn(nbIM)(nIM)	<i>gme</i>	
ZIF-10	Zn(IM) ₂	<i>mer</i>		ZIF-90	Zn(Ica) ₂	<i>sod</i>	
ZIF-67	Co(MeIM) ₂	<i>sod</i>		ZIF-95	Zn(cbIM) ₂	<i>poz</i>	
ZIF-71	Zn(dcIM) ₂	<i>rho</i>		ZIF-100	Zn ₂₀ (cbIM) ₃₉ (OH)	<i>moz</i>	

**Fig. 2** Plot of pore diameter (d_p) vs. surface area for the GME ZIFs: C black, N green, O red, Cl pink, Br brown, Zn blue, tetrahedral [5] (color figure online)

mixture of 1 Zn(NO₃)₂·6H₂O:70 HMeIM:1238·H₂O at room temperature in less than 5 min with an ~80 % product yield. TEM and field-emission scanning electron microscopy (FE-SEM) images showed that the particles had a sharp hexagonal facets with a mean particle size of ~85 nm.

ZIF-8 was also prepared to be a composite material for separation and catalysis. Thompson et al. reported the effects of sonication on ZIF-8 nanoparticles during the formation of ZIF-8/Matrimid mixed-matrix membranes in

tetrahydrofuran (THF). Direct sonication produced a composite membrane with enhanced properties compared to the pure polymer material [32]. ZIF-8@SiO₂ core-shell microspheres were prepared by the controlled growth of ZIF-8 (shell) on a spherical carboxylate-terminated SiO₂ (core) [33]. Yang et al. [34] reported the in situ synthesis of ZIF-8/CNT (CNT = hydroxyl-functionalized carbon nanotube) with different CNT loadings. SEM and TEM revealed a grape bunch-like morphology of the composite material with the formation of a hierarchical pore structure with a crystal size of 15–25 nm. The direct coating of ZIF-8 particles onto a siliceous mesocellular foam (ZIF-8@MCF) was prepared using two different routes: plate-like ZIF-8 microparticles were formed in DMF, whereas sphere-like nanoparticles were formed in water. The nanoZIF-8 on MCF had a higher Brunauer, Emmett, Teller (BET) surface area (935 m²/g) than microZIF-8 particles on MCF (279 m²/g) [35]. Zhang et al. [36] reported the formation of magnetic Fe₃O₄ core-ZIF-8 shell microspheres (Fe₃O₄@ZIF-8) through the functionalization of Fe₃O₄ particles with poly(styrenesulfonate, sodium salt) followed by the crystallization of ZIF-8 from a reaction mixture of 0.76 Zn(NO₃)₂·6H₂O:7.58 HMeIM in methanol at 323 K using solvothermal method for 3 h. The synthesized ZIF-8 shell was continuous and uniform with a ~100 nm thickness, as confirmed by TEM. The crystallinity and porosity of Fe₃O₄@ZIF-8 were examined by XRD and BET surface area measurement.

Table 2 ZIF-8 synthesis studies

Synthesis method	Synthesis conditions			Textural property		Comments ^c	Ref.
	Solvent ^a	Temp. (°C)	Time (h)	S _{BET} (m ² /g)	V _{Pore} (cm ³ /g)		
Solvothermal/ Hydrothermal	DMF	140	24	1947	0.66	Synthesis study of ZIF-n Gas sorption	[1]
	Methanol	RT	24	1264	0.51	Adsorption of CO ₂ , CH ₄ , N ₂	[30]
	H ₂ O	RT	5 min	1079	0.31	Synthesis of ZIF-8 nanocrystals in aqueous system	[31]
	Methanol	RT	1	1710 ± 60	0.58 ± 0.03	Synthesis of ZIF-8 nanoparticles Ultrasonication to avoid Ostwald ripening	[32]
	Methanol	70	15 min	1652.9	0.77	Separation of CO ₂ /N ₂ Synthesis of ZIF-8@SiO ₂ HPLC separation	[33]
Microwave	Methanol	90	6	1839	0.74	Synthesis of ZIF-8/carbon nanotube composites	[34]
	DMF	140	24	279	0.9	Adsorption of CO ₂ from CO ₂ /N ₂ mixture	[35]
	H ₂ O	RT	30 min	935	0.64	Synthesis of micro/hano ZIF-8@MCF Preparation of mixed-matrix membranes	[7]
	DMF	140	3	646	0.23	Separation of ethanol/water Synthesis study (conventional vs. microwave)	[39]
	Methanol	100	4	1496	0.77	Synthesis of ZIF-8 membrane Selectivity for H ₂ with respect to other gases	[40]
Sono chemical	Ionic liquid [bmin]BF ₄	140	1	471	0.34	Comparison (conventional vs. microwave) Adsorption of CO ₂	[41]
	H ₂ O	120	30 min	1075	0.49	Synthesis study	[42]
	DMF	45–60 110 W	4–9	–	–	Comparison (conventional vs. sonochemical)	[16]
Mechano chemical	DMF	60 % ^b	2	1174	0.50	Synthesis scale-up (1 L) Knoevenagel reaction	[43]
	Ethanol, DMF, DEF	RT/30 Hz	0.08–1	–	–	Effect of solvent, reaction time and additive salts	[44]
	DMF	RT	30 min	–	–	LAG, time resolved XRD study	[45]
	No solvent	RT/100 rpm	3–240	390–1480	0.47–1.05	Effect of reaction time Comparison (conventional vs. mechanochemical)	[46]
	Ethanol	RT/40 Hz	30 min	1390	–	Substituting Zn with Ni	[47]
Dry-gel conversion	Ethanol	RT/40 Hz	30 min	–	–	Introduction of polyoxometallates (H ₃ PW ₁₂ O ₄₀ , H ₄ SiW ₁₂ O ₄₀ , H ₃ P ₀ O ₁₂ O ₄₀) on ZIFs	[48]
	H ₂ O (liquid phase)	120	24	1470	0.69	Adsorption of methylene blue ZIF-8 as additives to liquid lubricants	[48]

Table 2 continued

Synthesis method	Synthesis conditions			Textural property		Comments ^c	Ref.
	Solvent ^a	Temp. (°C)	Time (h)	S _{BET} (m ² /g)	V _{Pore} (cm ³ /g)		
Oxide/hydroxide-based solvent-free	Solvent/additive-free	180	12	1450	0.56	Synthesis and CO ₂ adsorption study	[49]
Microfluidic	Solvent-free	100–160	–	1961	–	Synthesis study	[50]
	Methanol	50	5 min	–	–	Synthesis of Fe ₃ O ₄ @ZIF-8 magnetic core-shell microspheres Knoevenagel reaction	[51]
Electro chemical	H ₂ O	RT	1	–	–	Controlling particle size, N ₂ gas adsorption	[52]
	DMF, Methanol, Ethanol, H ₂ O	RT	10 min	1262–1695	0.56–0.66	Effect of the solvent, temperature and current density	[53]

^a DMF(*N,N*-dimethylformamide); [bmim]BF₄(1-butyl-3-methyl-imidazolium tetrafluoroborate); DEF(*N,N*-diethylformamide)

^b % sonication power

^c MCF siliceous mesocellular foams, LAG liquid-assisted grinding

The material showed a significantly lower BET surface area (430.9 m²/g) than pure ZIF-8 (1,643 m²/g). The magnetic Fe₃O₄@ZIF-8 particles were separated out within 10 s by an external magnetic field (14,000 Gs). Jin et al. reported the growth of ZIF-8 on a polyimide substrate by immersing the polyimide membrane into a reaction mixture of Zn(NO₃)₂·6H₂O:2 HMeIM in methanol at 298 K for 24 h. The resulting ZIF-8 crystals exhibited a rhombic dodecahedron morphology [37]. The semiconductor-MOF nanocomposite, Zn₂GeO₄/ZIF-8, was prepared by the in situ deposition of ZIF-8 on Zn₂GeO₄ nanorods by introducing the as-prepared Zn₂GeO₄ nanorods into a mixture of Zn(NO₃)₂·6H₂O and HMeIM in methanol [38]. High-magnification field-emission scanning electron microscopy (FE-SEM) showed that the size of the ZIF-8 nanoparticles on Zn₂GeO₄ nanorods was in the range, 10–50 nm.

Table 3 lists the solvothermal synthesis conditions of other ZIF structures as well as comments made on their synthesis [1, 3, 5, 12, 55–69].

2.2 Microwave Synthesis

Microwave-assisted synthesis techniques have been applied widely for the rapid synthesis of nanoporous materials under hydrothermal conditions. Besides fast crystallization, the technique can offer phase selectivity, a narrow particle size distribution, and facile morphology control because the microwave energy can be absorbed directly and uniformly throughout the entire volume of an object. Microwave synthesis equipment is typically consists of power output control and fiber optic temperature and pressure sensors [25, 70, 71].

Park et al. [39] evaluated the microwave synthesis of ZIF-8, and confirmed a decrease in crystal size (10–20 vs. 50–150 μm) and a significant reduction in the synthesis time compared to solvothermal electric heating. ZIF-8 was also prepared by microwave synthesis in methanol, and the synthesis protocol was applied to ZIF-8 membrane synthesis. A crack-free, dense polycrystalline layer of ZIF-8 crystals on top of the ceramic supports could be obtained by in situ crystallization [7]. Microwave synthesis was also carried out in the presence of an ionic liquid, 1-butyl-3-methyl-imidazolium tetrafluoroborate ([bmim]BF₄) [40]. A comparison with ZIF-8 prepared by conventional heating showed a more uniform morphology and improved specific surface area (471 vs. 341 m²/g). Bao et al. [41] reported the microwave synthesis of ZIF-8 under aqueous conditions at a substrate molar ratio of HMeIM/Zn²⁺ = 20.

2.3 Sonochemical Synthesis

Sonochemical synthesis involves the introduction of high-energy ultrasound to a reaction mixture, which can lead to

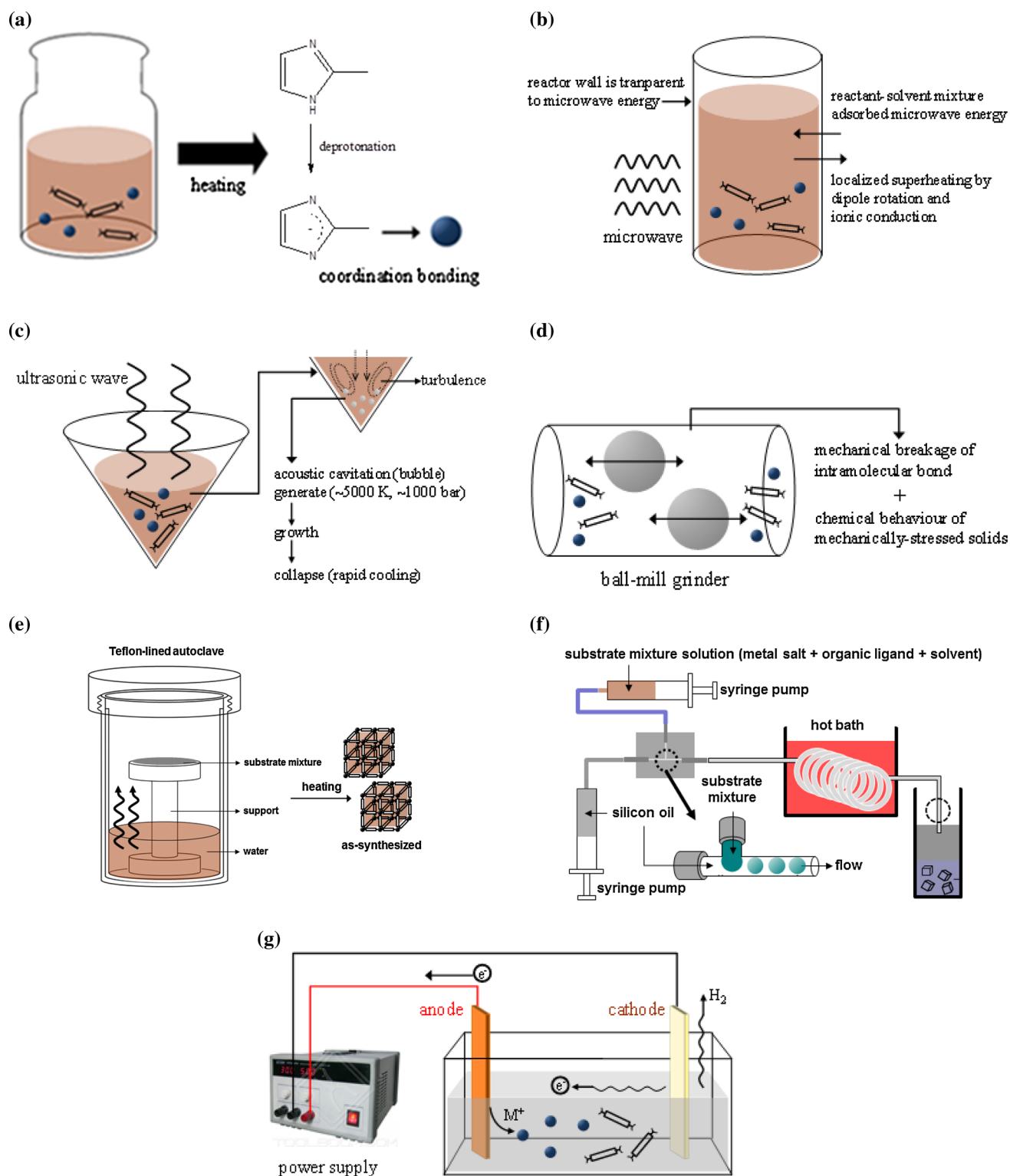


Fig. 3 ZIFs synthesis by **a** solvothermal, **b** microwave, **c** sonochemical, **d** mechanochemical, **e** dry-gel conversion, **f** microfluidic, and **g** electrochemical method [54]

rapid and homogeneous nucleation and result in a decrease in crystallization time and smaller/uniform particle size compared to those by conventional solvothermal synthesis.

The enhanced kinetics in sonochemical synthesis results from the formation and collapse of bubbles in the solution, which is termed acoustic cavitation, which produces very

Table 3 Solvothermal synthesis of ZIF-n

Sample	Synthesis conditions					Comments	Ref.
	Metal	Ligand	Solvent ^a	Temp. (°C)	Time (h)		
ZIF-9	Co(NO ₃) ₂ ·6H ₂ O	HbIM	DMF	130	48	Catalytic oxidation of aromatic oxygenates Knoevenagel reaction Tetralin oxidation	[5, 11, 25]
ZIF-10	Zn(NO ₃) ₂ ·4H ₂ O	HIM	DMF	85	96	Gas sorption Knoevenagel reaction	[1]
ZIF-67	Co(OAc) ₂	HMeIM	e-urea/ Ethanol	140	168	Cu doping Performance of visible-light-driven photocatalytic degradation	[56]
ZIF-71	Zn(OAc) ₂ Zn(OAc) ₂ ·2H ₂ O ZnO	HdcIM	Methanol	RT	24	Adsorption of EtOH and H ₂ O	[57]
			DMF	85	12	Adsorption of CO ₂	[58]
			Methanol	RT	24	Synthesis of mixed matrix membranes	[59]
			Methanol	RT	2	Synthesis of a ZIF-71 membrane	[60]
			Methanol	105	12	Separation of MeOH-H ₂ O, EtOH-H ₂ O, and DMC-MeOH	
			DMF	105	12		
ZIF-76	Zn(NO ₃) ₂ ·6H ₂ O	HIM/HcbIM	DMF/DEF	90	120	Adsorption of CO ₂ , CH ₄ , and N ₂	[61]
ZIF-78	Zn(NO ₃) ₂ ·4H ₂ O Zn(NO ₃) ₂ ·6H ₂ O	HnIM/ HnbIM	DMF	100	96	Selective adsorption of CO ₂	[5]
			DMF	120	48	Effect of the substrates concentration and HnIM/HnbIM ratio, Adsorption of CO ₂	[62]
			DMF	120	24	Synthesis of ZIF-78 membrane H ₂ /CO ₂ separation	[63]
			DMF	RT	5 min	Synthesis of ZIF-78 membrane Separation of cyclohexanone/cyclohexanol	[64]
ZIF-90	Zn(NO ₃) ₂ ·4H ₂ O	Ica	DMF	100	16	Bonding of ZIF-90 to fibers	[65]
			DMF	100	18	Post-synthesis functionalization of ZIFs	[66]
	Zn(NO ₃) ₂ ·6H ₂ O		H ₂ O/ Methanol	RT	1	Post-modification and fabrication of ZIF-8 for OT-CEC application	[67]
			DMF	RT	–	Synthesis of membranes Separation of H ₂ and CO ₂	[68]
	Zn(NO ₃) ₂		H ₂ O	RT	Few min	Particle size control	[69]
		H ₂ O/Alcohol ^b	RT				
	Zn(NO ₃) ₂ ·6H ₂ O		DMF/MeOH	RT	30 min		
ZIF-95	Zn(NO ₃) ₂ ·4H ₂ O	HcbIM	DMF/H ₂ O	120	–	Selective capture of CO ₂ from gas mixtures	[3]

HbIM, Benzimidazole; HdcIM, 4,5-dichloroimidazole; HIM, imidazole; HcbIM, 5-chlorobenzimidazole; HnIM, 2-nitroimidazole; HnbIM, 5-nitrobenzimidazole; ICA, imidazolate-2-carboxyaldehyde

OT-CEC Open tubular capillary electrochromatography

^a e-urea: ethyleneurea hemihydrate

^b Ethanol, propan-2-ol, isobutanol or *tert*-butanol

high local temperatures and pressures of approximately 5,000 K and 100 MPa, respectively, resulting in extremely rapid heating and cooling rates greater than 10¹⁰ K/s [25, 72].

The sonochemical synthesis of ZIF-8 enabled a decrease in synthesis time as well as synthesis at lower temperatures (318–333 K) compared to the solvothermal method (413 K). Smaller particles with a more uniform size distribution were obtained [42]. ZIF-8 was also prepared in the presence of NaOH (aq) or triethylamine (TEA) additive

under pH-adjusted synthesis conditions using a sonochemical method. Inexpensive industrial grade DMF was used as the solvent. A small amount of TEA, as a deprotonating agent, was necessary for obtaining ZIF-8 crystals, ~700 nm in size, which was approximately 400 times smaller than the ZIF-8 prepared by solvothermal synthesis. Sonochemical synthesis was carried out successfully in a 1 L batch scale-up and its pellet form was obtained using polyvinyl alcohol (PVA) as a binder [16].

2.4 Mechanochemical Synthesis

In mechanochemical synthesis, the mechanical breakage of intramolecular bonds was followed by a chemical transformation [73–75]. Mechanochemical synthesis can be carried out at room temperature (RT) under solvent-free conditions, which has the advantage of avoiding organic solvents in the synthesis [54]. The method offers a short reaction time (normally in the range of 10–60 min), which leads to quantitative yields and products comprised of small particles are generally obtained [25]. In many cases, a metal oxide is used as the substrate and water is produced as the sole byproduct [76]. The addition of small amounts of solvent, what is called liquid-assisted grinding (LAG), leads to the acceleration of mechanochemical reactions due to increases in the mobility of the reactants on the molecular level. The liquid introduced can also function as a structure-directing agent [25, 54]. Beldon et al. [43] first reported the mechanochemical synthesis of ZIFs, which involved the direct and topologically selective conversion of ZnO into porous and nonporous ZIFs based on imidazole (HIM), 2-methylimidazole (HMeIM) and 2-ethylimidazole (HEtIM) as the starting materials within a 30–60 min reaction time. Table 4 lists the results of the investigation. LAG was found to accelerate the formation and control the phases formed, and the synthesis of ZIFs was promoted in the presence of ammonium ions [43, 54]. The same group also reported the real-time study of mechanochemical transformations in a ball mill by the in situ diffraction of high-energy synchrotron X-ray analysis [44]. Tanaka et al. also reported the mechanochemical conversion of ZnO to ZIF-8, in which ZnO and HMeIM in a 300 mL ceramic pot were ground by a ball milling at a rotation rate of 100 rpm. All the reactions were performed on a 0.1 mol scale, and ZIF-8 was synthesized after 96 h with a BET surface area and micropore volume of 1480 m²/g and 0.55 cm³/g, respectively [45]. Recently, Li et al. prepared Ni-substituted ZIF-8 [46] and polyoxometallate (POM)-encapsulated ZIF-8 [47] by mechanochemical dry conversion.

2.5 Dry-Gel Conversion Synthesis

Dry-gel conversion (DGC) synthesis has been applied to the production of zeolites and zeolite membranes, in which the conversion of a dry amorphous aluminosilicate gel into a crystalline zeolite occurs by contacting with the vapors of water and volatile amines [77, 78]. DGC may also be useful for fabricating monolithic or shape-controlled porous materials from pre-shaped gels [79].

Recently, Dong et al. reported the dry-gel conversion synthesis of ZIF-8. ZIF-8 was prepared by placing Zn(OAc)₂·2H₂O (0.5 mmol) and HMeIM (5 mmol) on a small Teflon plate inside a Teflon-lined stainless steel

Table 4 ZIF topologies obtained in mechanochemical screening^a [43]

Ligand	Liquid	Salt			
		None	NH ₄ NO ₃	NH ₄ MeSO ₃	(NH ₄) ₂ SO ₄
HIM	None	Mixture ^b	zni	zni	Mixture ^b
HIM	DMF	cag	cag	Unknown ^d	cag
HIM	DEF	– ^c	nog	zni	Unknown ^d
HIM	EtOH	zni	zni	SOD	zni
HMeIM	None	–	SOD	SOD	–
HMeIM	DMF	SOD	SOD	SOD	SOD
HMeIM	DEF	SOD	SOD	SOD	SOD
HMeIM	EtOH	SOD	SOD	SOD	SOD
HEtIM	None	–	qtz	RHO ^e	–
HEtIM	DMF	–	qtz	ANA	RHO
HEtIM	DEF	–	qtz	ANA	RHO
HEtIM	EtOH	–	qtz	qtz	RHO

^a Each product was obtained by grinding for 30 min, – indicates no reaction

^b Mixture of starting materials, zni-type ZIF and an as yet unidentified material characterized by reflections in the 2θ range 10°–20°

^c No reaction is evident initially, but 24 h aging leads to cag- or nog-type ZIFs

^d Initial product is an as yet unidentified material, characterized by a reflection at 5.6°, which transforms into the nog-type ZIF on 24 h aging

^e Forms the qtz-type ZIF on 7 days aging

autoclave. H₂O (2.0 mL) was added to the bottom of the autoclave, and heated to 393 K and kept for 24 h. TGA of ZIF-8 (or ZIF-67) obtained by the DGC method showed that the H₂O guest molecule was removed much more easily from the narrow six-ring pore of the *sod* cage than organic DMF [48].

2.6 Oxide/Hydroxide-Based Solvent-Free Synthesis

Lin et al. [49] reported the synthesis of ZIF-8 without a solvent or additive by heating a reaction mixture of metal oxide or hydroxide and imidazolate ligands. In a typical synthesis, ZnO (2.5 mmol) and HMeIM (5 mmol) were ground and heated to 453 K for 12 h in ~100 % yield. The BET surface area and micropore volume were 1,450 m²/g and 0.56 cm³/g, respectively, without the necessity of washing or high-temperature treatment. The method may allow the large scale production of ZIF-8 for industrial use through ecologically more acceptable processes, including a high product yield (nearly 100 %) and the minimization of by-product formation (water as by-product). The authors suggested the space–time yield (STY: kilograms of product per cubic meter of reaction mixture per day) of 1400 kg/m³ day is feasible. Lanchas et al. described the

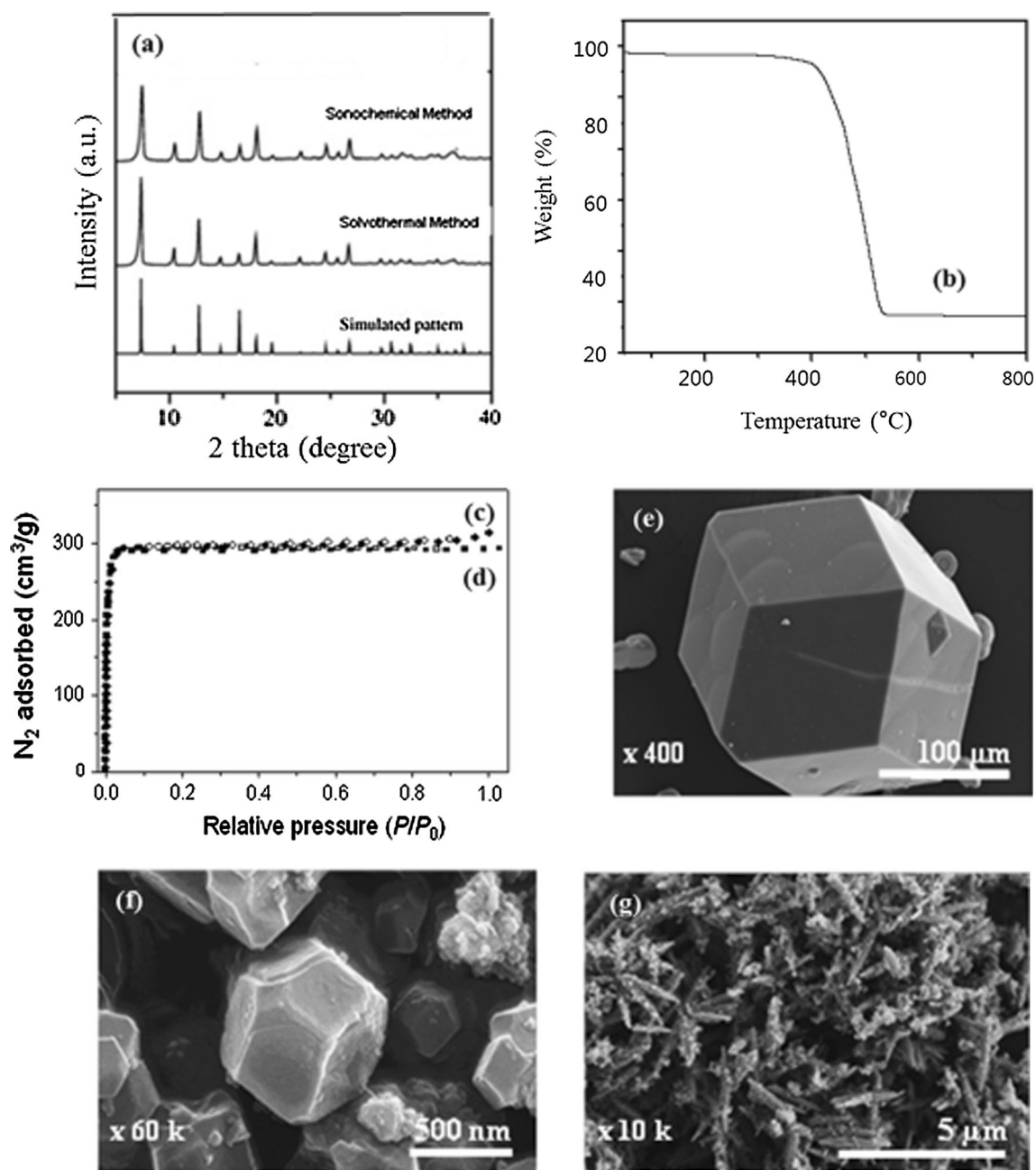


Fig. 4 Characterization for ZIF-8: **a** XRD patterns of observed and simulated one from the crystallographic information in Refs. [1, 16]; **b** TGA profile; N_2 adsorption–desorption isotherms (at 77 K) from **c** solvothermal and, **d** sonochemical method (the *filled-symbols* are

adsorption and *blank-symbols* are desorption); SEM images from **e** solvothermal method, **f** sonochemical method using triethylamine, **g** sonochemical method in the absence of triethylamine [16]

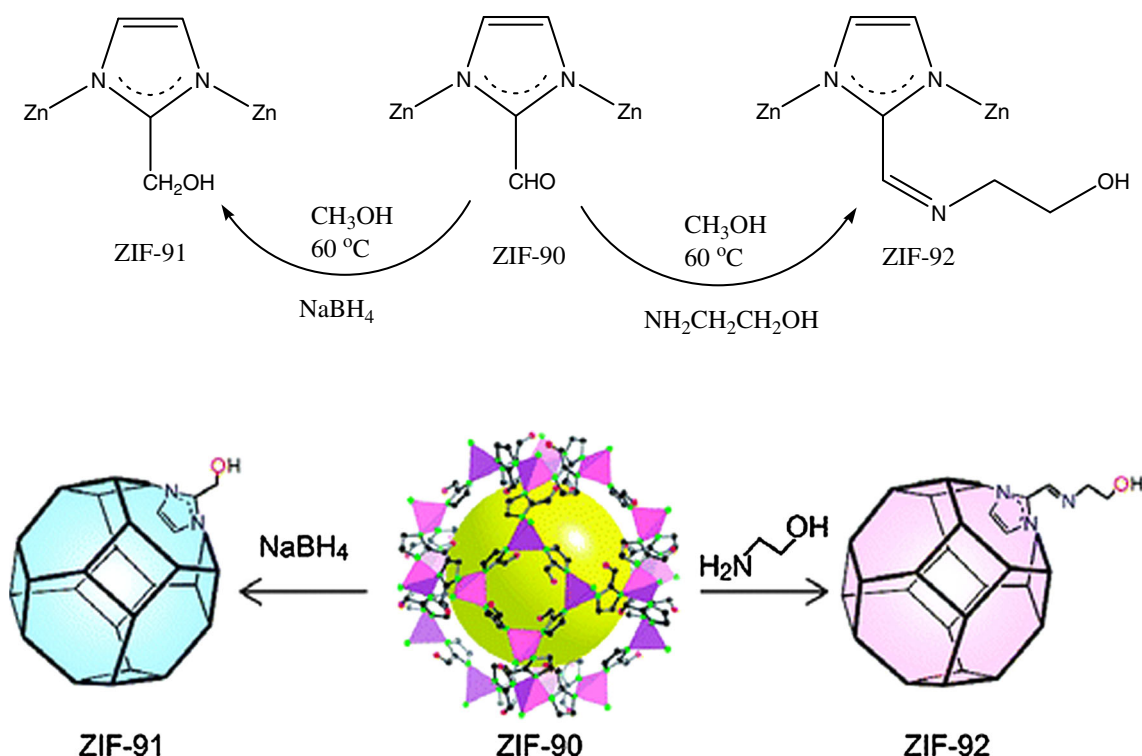
synthesis of ZIFs by heating (373–433 K) the metal oxide or hydroxide and imidazolate ligands using structure-directing agents

(1-butanol, pyridine and 4-methylpyridine) under solvent-free conditions, in which the reaction mixture of Zn:ligand:structure-directing agent (1:2.1:2.5) was used to obtain ZIF-8 and its related structures in 87–97 % yield [50]. They reported that the crystallinity, mean crystal size, and

network topology depended on the synthetic conditions, such as the heating rate and structure directing agent.

2.7 Microfluidic Synthesis

In general, microfluidics can be defined as systems that process or manipulate minute (10^{-9} – 10^{-18} L) amounts of fluids through channels with diameters in the range of tens of



Scheme 3 Preparation of ZIF-91 and ZIF-92 via post-synthesis functionalization of ZIF-90 [66]

hundreds of micrometers [80]. Both immiscible liquids are injected to a T-junction by syringe pumps, where aqueous solution droplets are formed in a continuous organic phase. The flow rates of both solutions can be adjusted independently. The capsule shell is formed at the liquid–liquid interface while these droplets pass through the hydrophobic tubing [81]. A microreactor has the advantage of rapid mixing, which offers a homogenous reaction condition and is effective for diffusion-controlled reactions [51].

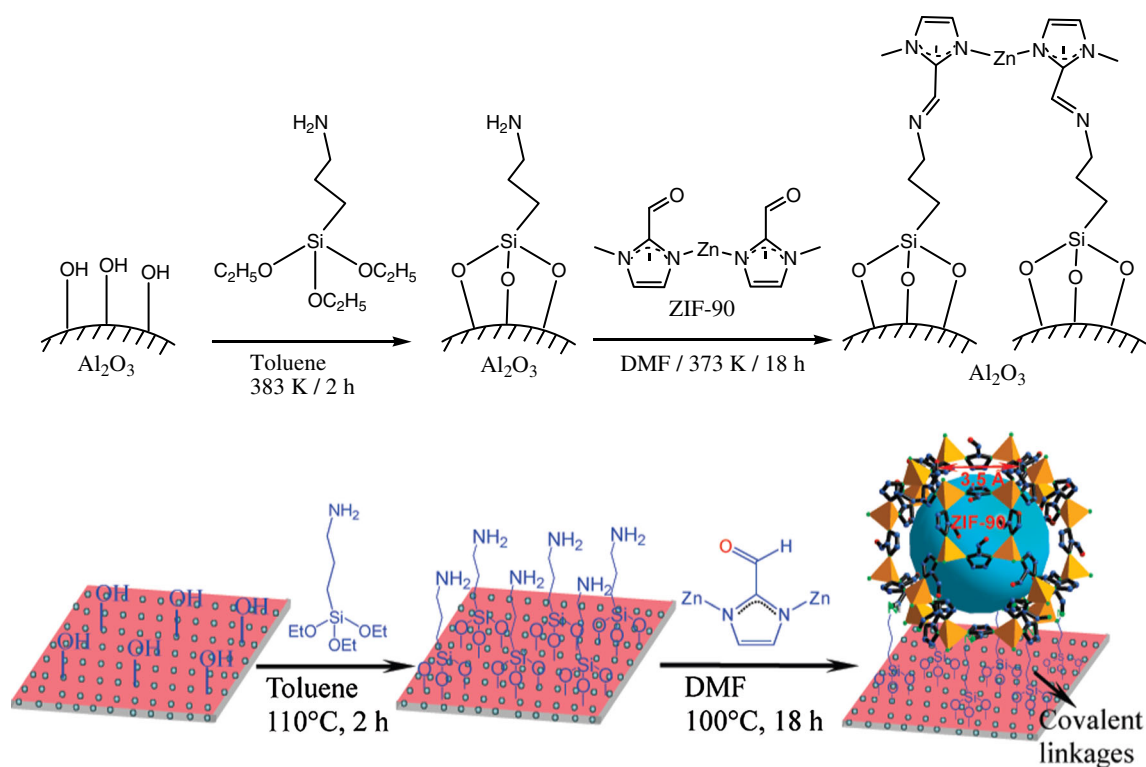
Yamamoto et al. [52] reported the microfluidic synthesis of ZIF-8. The preparation of ZIF-8 nanoparticles occurred in an excess of HMeIM to accomplish the rapid coordination reaction. An aqueous HMeIM solution at various concentrations and an aqueous 0.05 M ZnNO_3 solution were mixed using a T-type micromixer at various temperatures. The flow rates (HMeIM solution: ZnNO_3 solution = 1:1) ranged from 1 to 40 mL/min, which was controlled using a syringe pump. Recently, Faustini et al. [51] reported the microfluidic synthesis of Fe_3O_4 @ZIF-8 magnetic core–shell microspheres. Microfluidic droplets were formed by injecting a Fe_3O_4 precursor solution and oil phase, and heating the combined phases at 353 K for 2 min. The generated in-droplet Fe_3O_4 particles were then transported downstream to the second microreactor to merge with a mixture of ZIF-8 precursor (i.e., $\text{Zn}(\text{NO}_3)_2 \cdot 6\text{H}_2\text{O}$ and HMeIM dissolved in methanol) and polystyrenesulfonate for the synthesis of the

ZIF-8 shell at 323 K. The composite material, Fe_3O_4 @ZIF-8, showed the characteristic diffraction XRD peaks of both ZIF-8 and Fe_3O_4 . SEM further confirmed the presence of a ZIF-8 shell on the core magnetic particle (size range 700 ± 50 nm).

2.8 Electrochemical Synthesis

Electrochemical synthesis has several advantages: (1) faster synthesis at lower temperatures than conventional synthesis; (2) metal salts not required, and thus the separation of anions, such as NO_3^- or Cl^- from the synthesis solution is unnecessary; and (3) the total utilization of the linker can be achieved [53]. The basic synthesis principle involves supplying the metal ion by anodic dissolution to a substrate mixture containing the organic linker and an electrolyte. However, the method liberates H_2 during the electrochemical synthesis originated from the dissolved organic linker molecules.

ZIF-8 was synthesized by anodic dissolution in an electrochemical cell [53]. The ZIF-8 was prepared using DMF, H_2O -acetonitrile (AcN), MeOH, H_2O , mixture of H_2O and MeOH as the solvent, tributylmethylammonium methyl sulfate (MTBS), and KCl as the electrolyte. The DMF/MTBS couple resulted in high synthesis efficiencies under mild reaction conditions (RT, 10 min).



Scheme 4 Preparation of ZIF-90 membrane on 3-aminopropyltriethoxysilane modified Al_2O_3 support [82]

3 Characterization of ZIF-8

The MOF materials are characterized routinely by XRD (structure identification), SEM (morphology), N_2 adsorption–desorption isotherms (textural properties of surface area/pore volume), and TGA (structural stability). A range of spectroscopic techniques and elemental analysis are also used to characterize the new materials to identify the organic functional groups and confirm the chemical compositions.

As shown in Fig. 4a, the powder XRD pattern of the synthesized materials must be in good agreement with that of the XRD pattern simulated from the crystallographic information of the ZIF structure. The thermal stability of the material was measured by TGA. As shown in Fig. 4b, a one-step weight change was observed; a sharp weight loss between 673 and 823 K due to decomposition of the network, and no further weight loss occurred up to 1,073 K [16]. The N_2 adsorption–desorption isotherms of both materials (prepared using sonochemical and solvothermal methods) represented in Fig. 4c and d showed a type I isotherm, which reflects the microporous network of ZIF-8. The BET surface area and total pore volume of ZIF-8 were ca. $1,174 \text{ m}^2/\text{g}$ and ca. $0.5 \text{ cm}^3/\text{g}$, respectively. SEM (Fig. 4e–g) showed that the morphology and particle size of ZIF-8 can vary according to the synthesis method. Both images showed well-shaped high quality typical polyhedral crystals with a variable size, which had been obtained

using sonochemical or conventional solvothermal methods. The sonochemical method, however, produced a much smaller particle size (ca. 700 nm) than the conventional solvothermal method (ca. 250 nm). A change in morphology to needle-shaped particles was observed using NaOH as the deprotonating agent in the reaction mixture, as shown in Fig. 4g.

4 Functionalization

The functionalization of ZIFs is often necessary for many catalytic/adsorption applications. ZIF-8 and ZIF-90 structures are prominent in this respect. This section will also cover post-synthesis functionalization/modification and noble metal deposition.

Yaghi et al. [66] reported the synthesis of ZIF-90 using carboxaldehyde-2-imidazole as a linker to achieve a chemical composition of $\text{Zn}(\text{C}_4\text{H}_3\text{N}_2\text{O})_2$. ZIF-90 exhibited a *sod* topology with an aperture, 3.5 Å in diameter and 11.2 Å in pore size. The BET surface area was $1,270 \text{ m}^2/\text{g}$ and showed high thermal and chemical stability. ^{13}C cross polarization magic angle spinning nuclear magnetic resonance (NMR) and Fourier transform infrared (FTIR) spectroscopy confirmed the aldehyde group in the ZIF-90. The author reported the post-synthesis functionalization of ZIF-90 through reduction of the $-\text{CHO}$ group with NaBH_4

to alcohol and a condensation reaction with ethanolamine to an imine in methanol at 333 K to form ZIF-91 and -92, respectively (Scheme 3). XRD confirmed that the parent framework had been maintained after post-functionalization but the BET surface area of ZIF-91 ($S_{\text{BET}} = 1010 \text{ m}^2/\text{g}$) was lower than the parent ZIF-90 ($S_{\text{BET}} = 1270 \text{ m}^2/\text{g}$), and ZIF-92 showed a severely blocked pore aperture due to the presence of an imine group.

Huang et al. [82] reported the preparation of molecular sieve ZIF-90 membranes through a two-step process of (i) surface functionalization of porous Al_2O_3 using 3-aminopropyltriethoxysilane, and (ii) nucleation and crystallization of ZIF-90 from a reaction mixture of $\text{Zn}(\text{NO}_3)_2 \cdot 4\text{H}_2\text{O}$ and imidazolate-2-carboxyaldehyde in DMF at 373 K using a solvothermal method and condensation reaction of a $-\text{CHO}$ group with amine to imine for 18 h (Scheme 4). The material showed the characteristic XRD peaks of both ZIF-90 and Al_2O_3 , and the resulting ZIF-90 layer exhibited a rhombic dodecahedron morphology with a thickness of approximately 20 μm , as confirmed by SEM. The authors expanded the concept [83] and reported the post-synthesis functionalization of the as-synthesized ZIF-90 crystals and membranes by immersing the as-synthesized ZIF-90 crystals and membranes into 3-aminopropyltriethoxysilane in methanol at 383 K to form the organosilica-functionalized ZIF-90 membrane. Yu and Yan [65] similarly reported the covalent bonding of ZIF-90 to amino-functionalized silica fibers, and ZIF-90 was also immobilized on the capillary wall via condensation between the free aldehyde of the ZIF-90 and the amine group of 3-aminopropyltriethoxysilane [67].

A *sod* ZIF structure with $\sim 85\%$ un-substituted imidazolate linkers having a chemical composition of $\text{Zn}(\text{IM})_{1.7}(\text{MeIM})_{0.3}$ (HIM = imidazole and HMeIM = 2-methylimidazole) was prepared via the linker exchange of ZIF-8 in *n*-butanol at 373 K after 7 days. [84]. The size and morphology of the ZIF-8 crystals were unchanged during the reaction but the BET surface area of the material was lower than that of ZIF-8. Subsequently, the product was treated with *n*-butyllithium to form coordinated non-structural Li^+ ions at the C2 site, which acted as a Brønsted base for the conjugated addition reaction (discussed in Sect. 5.4).

Several synthetic strategies have been used to prepare nanoparticles supported on ZIF-8. Pd nanoparticles supported on ZIF-8 can be prepared from (i) an acetone solution of $\text{PdCl}_2(\text{CH}_3\text{CN})_2$ added to ZIF-8 and reduction by NaBH_4 at low temperatures to form Pd particles with various degrees of aggregation [85], or (ii) an aqueous solution of K_2PdCl_4 using polyvinyl alcohol as the stabilizer and hydrazine as the reducing agent to produce nanoparticles in the range, 4–9 nm, which are well dispersed on the external surface of ZIF-8 [17]. The BET

surface areas of ZIF-8 and Pd/ZIF-8 were almost identical, however, the possibility of a trace amount of polyvinyl alcohol remained on the surface of Pd/ZIF-8 cannot be ruled out. Wang et al. [86] reported the encapsulation of Pt nanoparticles in ZIF-8 by the nucleation of ZIF-8 nanostructures with pre-formed Pt nanoparticles (prepared from H_2PtCl_6 using the glycol reduction method) to produce nanoparticles in the range, 2–3 nm. ZIF-8-loaded TiO_2 nanotube composites were synthesized by the in situ growth of ZIF-8 on the TiO_2 nanotube layer with dimensions in the range, 20–40 nm. The resulting structure was immersed into a H_2PtCl_6 solution, followed by reduction using NaBH_4 to form Pt-supported ZIF-8 loaded on TiO_2 nanotubes [87].

Lu et al. [88] reported the encapsulation of Au, Pt and other semiconductor guests within ZIF-8 through functionalization of the nanoparticles surface with polyvinylpyrrolidone and the subsequent crystallization of ZIF-8 in methanol at room temperature for 24 h. The authors extended the synthesis route for the preparation of hybrid crystals with two types of nanoparticles distributed homogeneously, such as 13 nm Au nanoparticles and 34 nm Au nanoparticles, through the concurrent addition of two types of nanoparticles. A trace amount of polyvinylpyrrolidone was present in the resulting nanoparticle/ZIF-8 composites, as confirmed by TGA and BET surface area measurements.

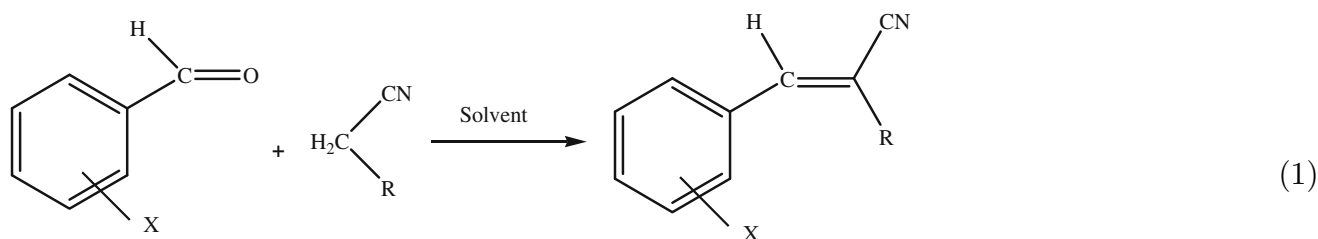
Zahmakiran [89] reported the encapsulation of iridium nanoparticles in ZIF-8 (Ir-ZIF-8) through a two-step process involving (i) gas phase infiltration of (methylcyclopentadienyl)(1,5-cyclooctadiene)iridium(I) into ZIF-8 and (ii) hydrogenolysis using H_2 (10 % H_2 :90 % N_2) at 573 K to produce nanoparticles in the range, 2.2–6.5 nm with a mean diameter of 3.3 ± 1.7 nm. High resolution TEM of Ir-ZIF-8 showed the highly crystalline nature of Ir nanoparticles with an ~ 0.23 nm interplanar spacing, and the iridium nanoparticles were well-dispersed within the ZIF-8 matrix. Ru-supported ZIF-8, Ru-ZIF-8, was prepared using a wet impregnation method from RuCl_3 salts using a range of impregnating solvents, such as ethanol, methanol, acetone, acetonitrile, and water [90]. TEM showed that the size of Ru species synthesized from ethanol and water solvent ranged from 1.0 to 1.5 nm.

Au nanoparticles supported on ZIF-8 and ZIF-90 were obtained by the gas phase infiltration of $[\text{Au}(\text{CO})\text{Cl}]$ into the activated ZIFs, followed by hydrogenation using H_2 (0.2 MPa) at 373 and 403 K for ZIF-8 and ZIF-90, respectively [14]. High-resolution TEM showed that the encapsulation of Au nanoparticles supported on ZIF-8 produced Au nanoparticle having a wide size distribution of 1–5 nm, where most were 2–4 times larger than the dimensions of the ZIF-8 cavity, whereas the encapsulated Au nanoparticles in ZIF-90 (Au-ZIF-90) exhibited very

small particles in the size range, 1–2 nm, which were distributed homogeneously throughout the interior of the ZIF-90 matrix, suggesting that the functional groups (–CHO) of ZIF-90 are responsible for forming the much

created through the functionalization of ZIF-8, which can act as the catalytic sites for various organic transformations.

5.1 Knoevenagel Condensation Reaction



X = 4-NO₂, 4-Cl, 4-CH₃, 3-CH₃, 2-CH₃.
R = CN or COOC₂H₅

smaller nanoparticles with a narrow size distribution (>95 %, ≤2 nm). Li et al. [91] reported the synthesis of Au and Ag nanoparticles onto ZIF-8 through a coordination interaction between the capping surfactants of metal nanoparticles and ZIF-8 to form Au and Ag particles size of 2–3 or 1–2 nm, respectively. ZIF-8 nanocrystals prepared using hexadecyltrimethyl ammonium bromide as the capping agent in a DMF or water medium produced two different morphologies, rhombic dodecahedron or cubic hexahedron with crystal sizes of ~70 and ~120 nm, respectively.

Jiang et al. [92] reported the preparation of Au@ZIF-8, Au@Ag/ZIF-8, Au@AuAg/ZIF-8 and Ag/ZIF-8 via the following sequential deposition-reduction route: (i) deposition of Au or Ag on ZIF-8 using HAuCl₄ or AgNO₃ salts, and (ii) reduction of Au or Ag using NaBH₄. Kuo et al. reported the synthesis of the yolk-shell of Pd nanocrystals onto ZIF-8 through (i) the coating of Pd octahedra using Cu₂O as the sacrificial template to form a Pd@Cu₂O core-shell structure, and (ii) Pd@Cu₂O core-shell reacts with a reaction mixture of Zn(NO₃)₂·6H₂O and HMeIM in a methanol medium to form Pd@ZIF-8 [93].

5 Heterogeneous Catalysis

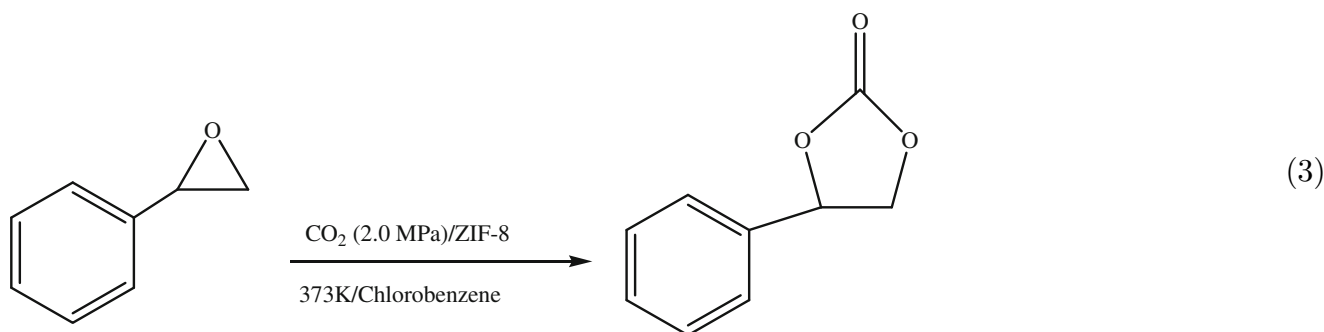
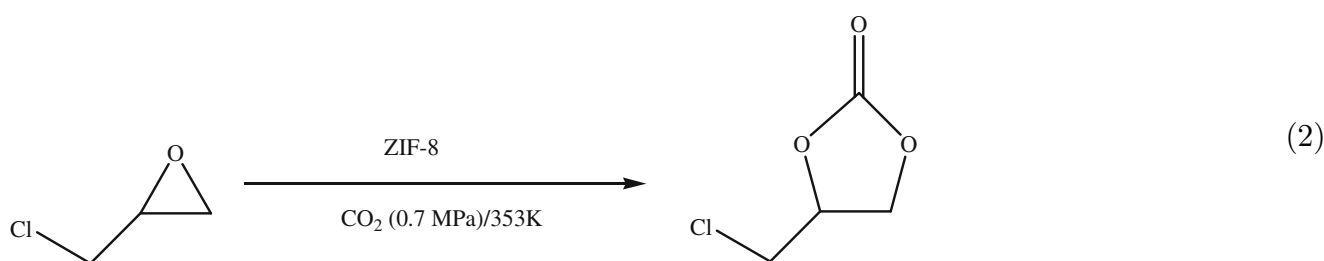
ZIFs are highly crystalline porous materials with high thermal and chemical stability. As listed below, many types of reactions (Lewis acid, Lewis base and Brønsted base catalyzed reactions as well as catalysis reactions by the ZIF-supported metal nanoparticles) have been reported using ZIF-8 and others including ZIF-9, -10, -67 and -90. The ZIF-8 framework, for example, contains Lewis acid Zn²⁺ and nitrogen base moieties, and the Brønsted base sites can be

ZIF-8 and functionalized ZIF-8 were applied to the Knoevenagel condensation reaction as a base-catalyzed model reaction (1) [16, 36, 37, 94]. Tran et al. [94] conducted rigorous catalytic tests to evaluate the catalytic properties of ZIF-8 for the condensation of benzaldehyde and malononitrile at room temperature. The catalyst exhibited high activity (100 % conversion after 2 h) using 4:1 (malononitrile:benzaldehyde molar ratio) and 5 mol% ZIF-8 catalyst in toluene. The conversion was found to be dependent on the reaction time, molar ratio of the reactant, and catalyst concentration. The catalyst with the smaller particle size afforded higher activity than the larger crystals, suggesting that the reaction occurred mainly on the external surface of the ZIF-8 crystal, where the catalytically active basic nitrogen atoms are located. ZIF-8 in THF resulted in higher activity than in toluene, whereas methanol was found to be an ineffective solvent for the Knoevenagel condensation reaction. An electron-withdrawing group attached to benzaldehyde in 4-nitrobenzaldehyde resulted in higher reactivity than the benzaldehyde derivatives with electron-donating groups. Hot filtration experiments and recycling running over the spent catalysts supported its heterogeneous reaction. Cho et al. [16] examined the Knoevenagel condensation reaction of benzaldehyde to malononitrile at 298 K using a ZIF-8 catalyst synthesized on a 1-L scale via the sonochemical route. The catalyst produced by the sonochemical route exhibited significantly higher activity than that prepared by the solvothermal method under identical reaction conditions. This suggests that the smaller catalyst size by the sonochemical route (700 nm) is better than that produced by the solvothermal route (250 μm). Zhang et al. reported the Knoevenagel condensation reaction of benzaldehyde

with ethyl cyanoacetate using Fe_3O_4 -ZIF-8 in a flow capillary micro reactor and showed good activity (100 % conversion) at 353 K after 25 min [36]. Faustini et al. [51] reported the microfluidic catalytic system for Knoevenagel condensation of benzaldehyde with ethyl cyanoacetate using Fe_3O_4 @ZIF-8 and ~99 % conversion was obtained at 353 K after 35 min. The magnetic Fe_3O_4 @ZIF-8 catalyst can be easily separated from the solution with negligible loss by applying external magnetic field. The ZIF-8 crystals on the electrospun polyimide nanofibers (~65 wt % ZIF-8) exhibited good catalytic activity (90-96 % conversion) in the Knoevenagel condensation reaction at 298 K after 12 h, but partial destruction of the catalyst was observed after recycle runs [37]. Nguyen et al. [55] reported the Knoevenagel condensation reaction of benzaldehyde with malononitrile using ZIF-9 at 298 K. The material exhibited high activity (99 % conversion after 2 h) in THF. Their work suggested that the high catalytic activity originated from the external surface of the ZIF-9 particles. They compared ZIF-8, ZIF-9 and ZIF-10 catalysts for the Knoevenagel condensation reaction, and the reaction rate decreased in the following order ZIF-9 < ZIF-8 < ZIF-10. ZIF-10 showed a higher reaction rate due to the less hydrophobic surface.

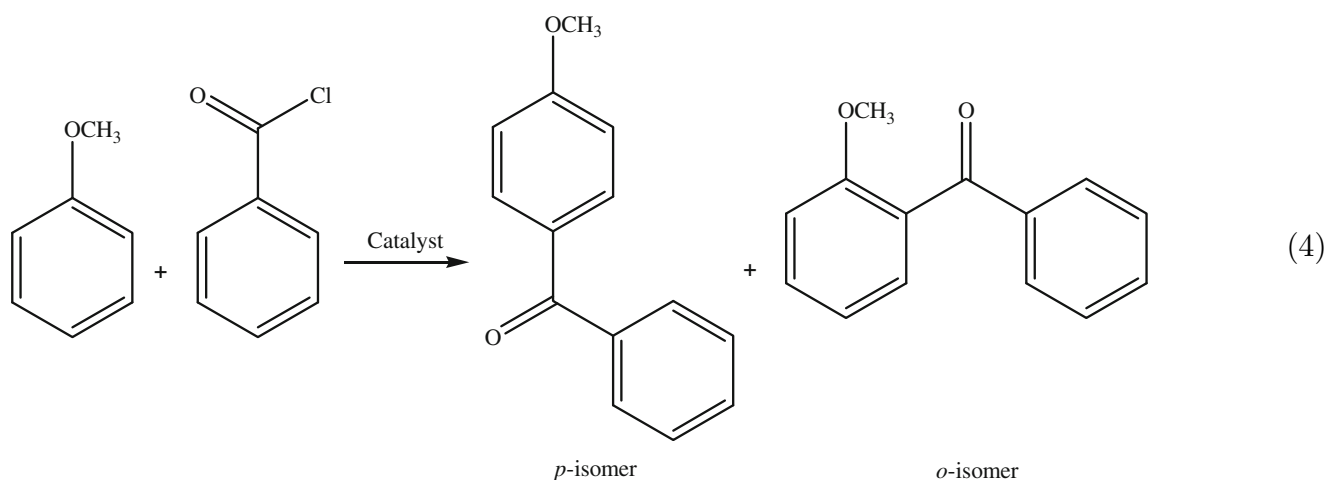
5.2 CO_2 Cycloaddition of Epoxides

ZIF-8 was applied to the Lewis acid/base-catalyzed cycloaddition of CO_2 to alkene oxide using high pressure CO_2 (0.7–2.0 MPa) [15, 95, 96]. Miralda et al. [15] reported the cycloaddition of CO_2 to epichlorohydrin over ZIF-8 and amine-functionalized ZIF-8 catalysts under solvent-free conditions as in (2). The amine-functionalized ZIF-8 (grafting of ethylenediamine to ZIF-8) exhibited higher conversion (100 %) and selectivity (73.1 %) to chloropropene carbonate than the non-functionalized ZIF-8 (84.1 % conversion and 52.0 % selectivity to chloropropene carbonate). In both catalysts, the conversion increased gradually and the selectivity to chloropropene carbonate decreased when the temperature was increased from 343 to 373 K. The highest chloropropene carbonate yield was obtained at 353 K. In the recycle runs, both ZIF-8 catalysts showed significantly lower activity than the fresh catalysts. The ZIF-8 structure was retained after the first recycle as confirmed by FTIR and XRD, but the BET surface area decreased substantially, suggesting active site pore blocking by the carbonaceous material formed during the reaction. For styrene oxide in (3), 39.4 % conversion and ~100 % selectivity to styrene carbonate were obtained using CO_2 at 0.7 MPa and 353 K after 5 h, but the yield of styrene carbonate from the fresh catalyst decreased upon recycling from 39.4 to 37 % after first and third recycle, respectively. XRD and SEM confirmed that the structure and morphological features of ZIF-8 were retained after the recycle runs [96]. It was proposed that the styrene oxide is activated on the Lewis



acid Zn^{2+} ions and CO_2 on the basic nitrogen atoms of the imidazole ligand, and the activated CO_2 is then inserted into the epoxide via nucleophilic attack forming the cyclic carbonate. The concurrent presence of Lewis acid Zn^{2+} and base nitrogen sites was desirable for high catalytic activity of this type of reaction.

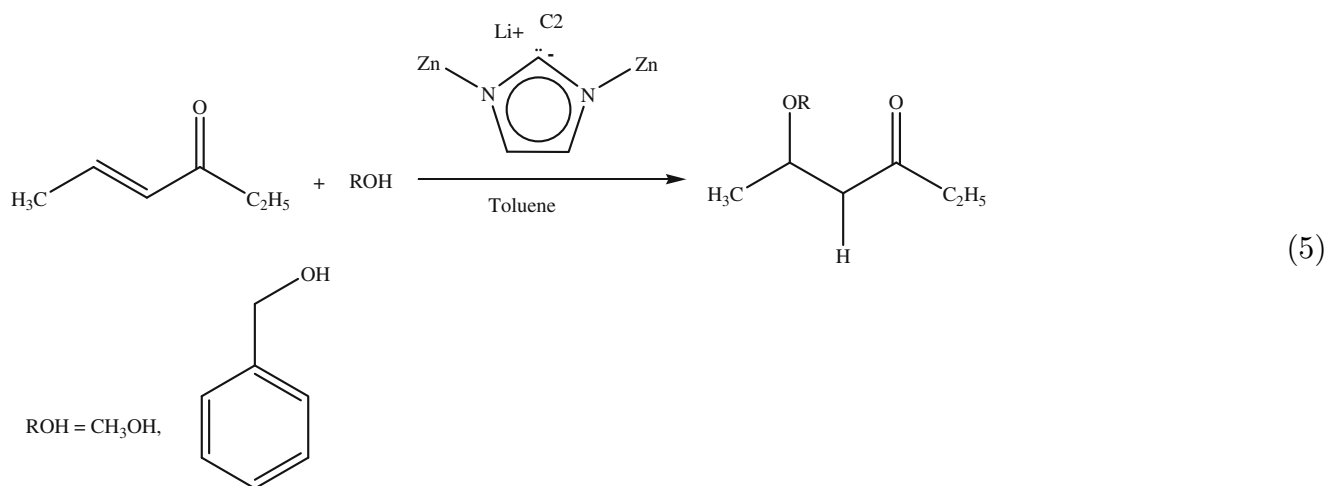
5.3 Friedel-Craft Acylation



ZIF-8 was applied to the Lewis acid-Brønsted acid-catalyzed Friedel-Craft acylation of anisole and benzoyl chloride in (4) under open air atmosphere conditions [97]. The conversion increased gradually from 36 to 58 % as the temperature was increased from 373 to 393 K, whereas the selectivity

to *p*-benzoylanisole remained relatively constant (93–95 %). The conversion increased with increasing catalyst amount from 2 to 6 mol%, and the conversion also increased from 69 to 92 % as the catalyst particle size decreased from 210 to 92 μm due to the increased external surface of the smaller crystals. 4-Methoxybenzoyl chloride showed higher conversion (87 %) than benzoyl chloride (82 %) or 4-chlorobenzoyl chloride (73 %) as an acylating agent, but exhibited lower selectivity to the product (*p*-isomer) under identical reaction

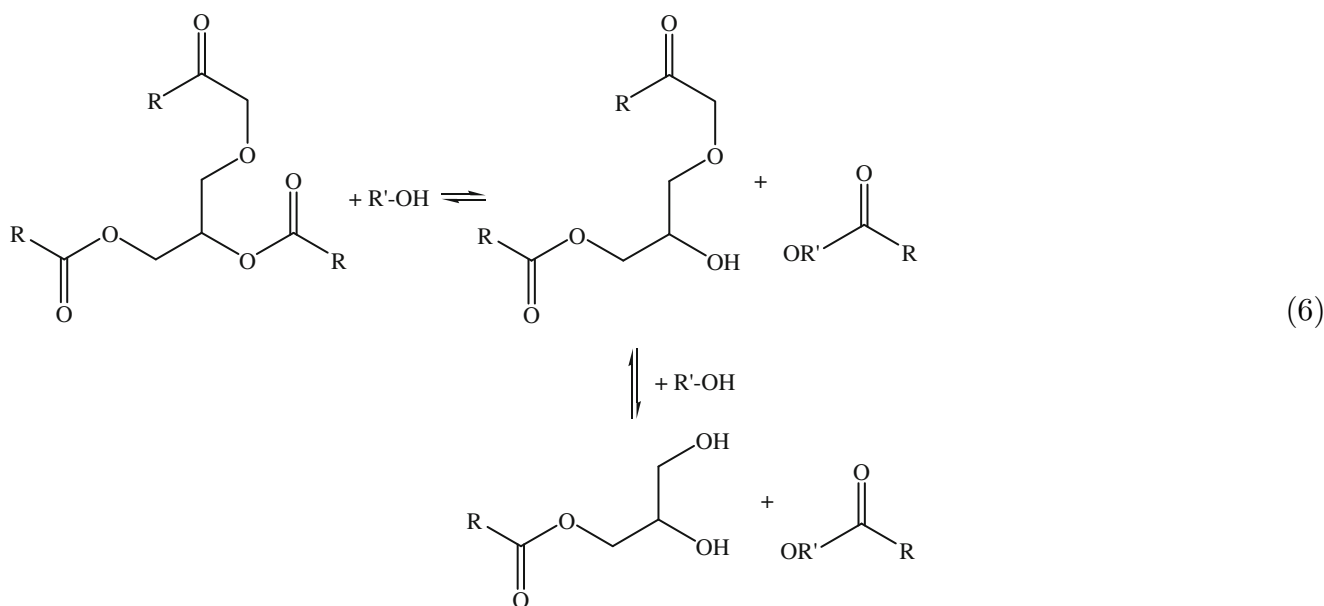
5.4 Conjugate-Addition Reaction



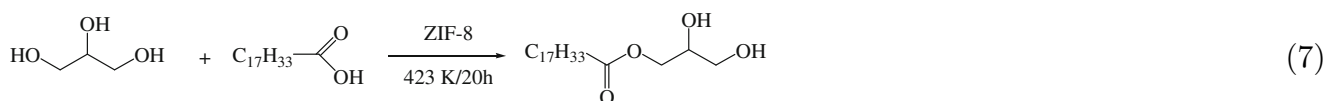
A unique ZIF structure with unsubstituted imidazolate linkers prepared by the solvent-assisted linker exchange of ZIF-8 and the subsequent introduction of n-butyllithium catalyzed the conjugated addition reaction in (5), in which methanol or benzyl alcohol and 4-hex-en-3-one were converted to the corresponding ether with a good yield (94 % conversion of methanol and 81 % conversion of benzyl alcohol) in toluene [84]. The catalytic activity originated from coordinated non-structural Li^+ ions, whereas the ZIF-8 catalyst containing a methyl group at C2 was not active. The heterogeneity of the catalyst was confirmed in a hot filtration experiment. XRD confirmed that the structure of the catalyst was unchanged during the reaction.

ZIF-8 was an efficient catalyst for the transesterification of vegetable oil using a range of alcohols (methanol, ethanol, 1-propanol, 1-butanol, isopropanol and tert-butanol) at 473 K as in (6) [13]. Methanol exhibited higher activity to monoglycerides (~ 100 % conversion at 473 K after less than 2 h) than the other alcohols, which correlated well with the acidity of linear alcohols. ZIF-8 showed better activity than conventional ZnAl_2O_4 catalyst. The reaction involves alcohol deprotonation and the activation of ester; alcohol is activated on the Lewis acid Zn^{2+} ions and base (OH or N^-) sites, whereas ester on the Zn^{2+} ions and Brønsted acid (NH) sites to form the product. This transesterification of vegetable oil suggested that the acidic-base active sites in ZIF-8 are located only on the external surface or at defects.

5.5 Transesterification of Vegetable Oil



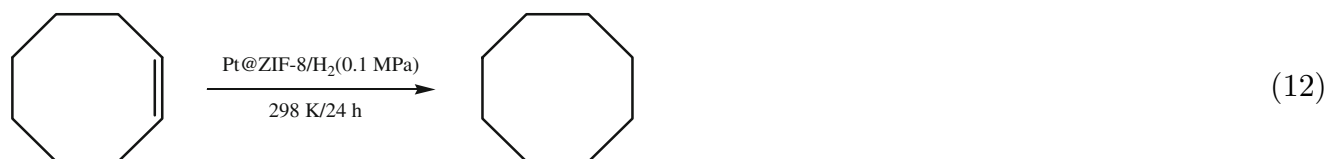
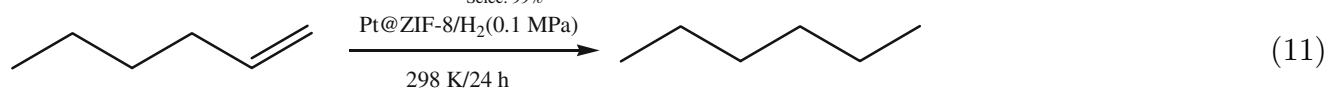
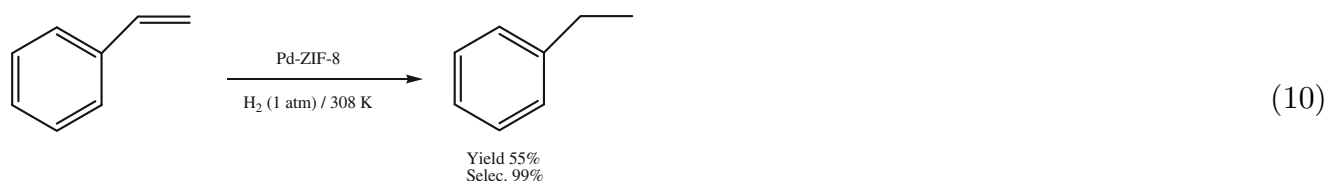
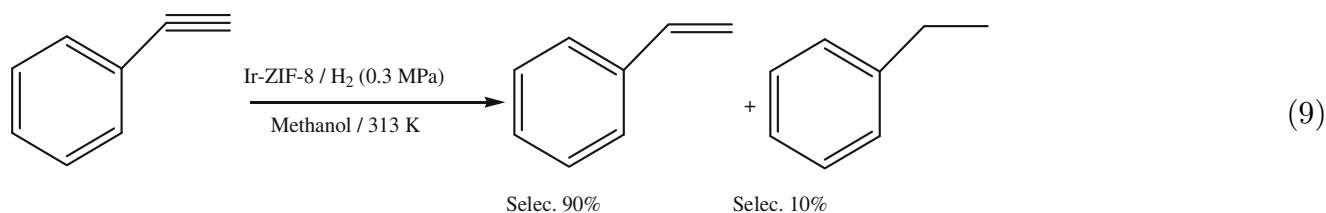
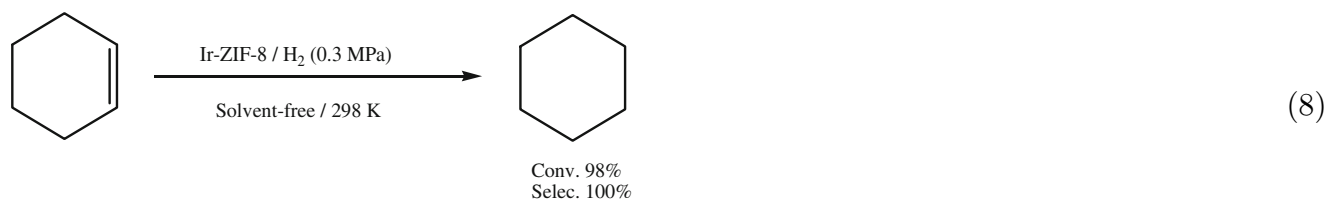
5.6 Esterification of Glycerol and Oleic Acid

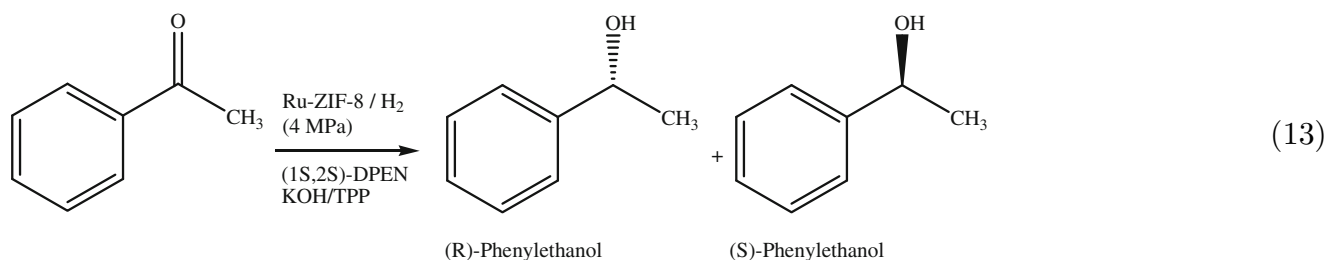


ZIF-8 was applied to an acid-catalyzed esterification reaction, and glycerol and oleic acid were converted to monoglyceride with 57 % conversion at 423 K after 20 h using *tert*-butanol in a batch reactor (7) [98]. The heterogeneity of the catalyst was confirmed using a hot filtration experiment, but small leaching of Zn (178–140 ppm) was detected in the filtrate solution. The combined TEM images and N₂ adsorption isotherms indicated that local framework restructuring occurred during the catalysis reaction to form mesopores, and the resulting hierarchical structure with the intrinsic micropores could be responsible for the catalytic activity.

The Ir, Pd, Pt, and Ru nanoparticles supported on ZIF-8 were applied to the hydrogenation reaction using molecular H₂ [85, 86, 88, 89, 93]. The Ir nanoparticles supported on ZIF-8 exhibited high activity (~98 % conversion) and selectivity (100 %) in the solvent-free hydrogenation of the cyclohexene in (8) at room temperature using H₂ (0.3 MPa) after 12 h [89]. In methanol, the material also showed good activity in the hydrogenation of phenylacetylene in (9) with 100 % conversion and 90 % selectivity to styrene after 16 h. The catalyst could be reused several times without losing its initial catalytic activity, and XRD and TEM confirmed that the crystallinity of Ir-ZIF-8 had been retained during the reaction with no leaching or agglomeration observed. The hydrogenation of styrene over the Pd supported on ZIF-8 produced ethylbenzene in (10) occurred in 55 % yield and 99 % selectivity using H₂

5.7 Hydrogenation of Alkene, Alkyne and Aromatic Ketone

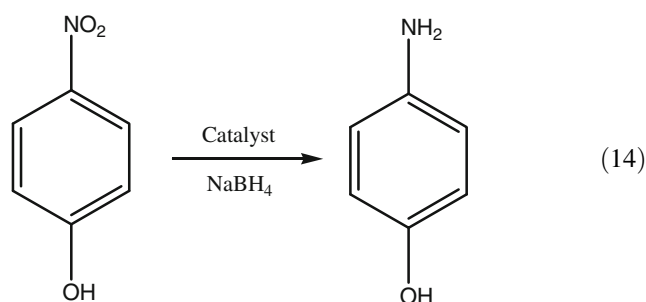




(1 atm) at 308 K [85]. Wang et al. [86] reported the hydrogenation of 1-hexene and cis-cyclooctene using a Pt nanoparticle-supported ZIF-8 catalyst in ethanol in (11) and (12). The smaller substrate, 1-hexene, converted to 1-hexane with 95 % conversion and 100 % selectivity at 298 K after 24 h, whereas the larger substrate, cis-cyclooctene exhibited only 2.7 % conversion. In 1-hexene hydrogenation, Pt nanoparticle-supported ZIF-8 catalyst showed much higher activity than the commercially available Pt on carbon under identical reaction conditions. XRD, FTIR, and TEM confirmed that the catalyst was reusable and stable under the reaction conditions. The asymmetric hydrogenation of acetophenone in the presence of an achiral modifier triphenylphosphine (TPP) and chiral modifier (1S,2S)-1,2-diphenylethylenediamine [(1S,2S)-DPEN] as in (13) over a range of Ru-ZIF-8 catalysts prepared from different impregnation solvents were reported [90]. The catalyst prepared in ethanol showed higher conversion (96.7 %) and ee (67.1 %) than the one prepared in water (19.3 % conversion and 56.4 % ee) under similar reaction conditions. The heterogeneous nature of the catalysts was confirmed from hot filtration experiments. The yolk-shell Pd-ZIF-8, core-shell Pd-ZIF-8 and Pd on ZIF-8 (in which Pd nanocrystals were deposited directly onto ZIF-8) were applied to the gas phase hydrogenation of ethylene, cyclohexene and cyclooctene with 100 Torr H₂ and 650 Torr He at 323 K [93]. The catalysts showed high activity in the hydrogenation of smaller substrates, ethylene and cyclohexene. No activity was observed in cyclooctene hydrogenation using both yolk-shell Pd-ZIF-8 and core-shell Pd-ZIF-8 catalysts because of the much larger size of cyclooctene (5.5 Å)

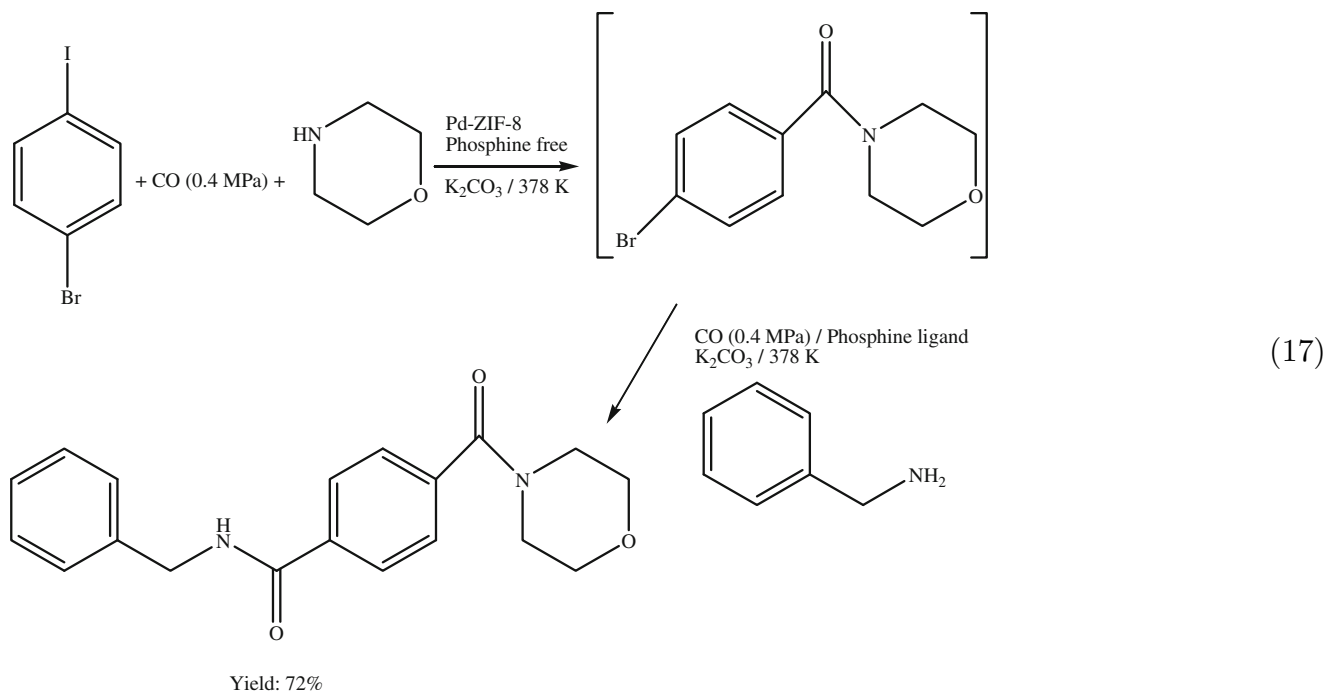
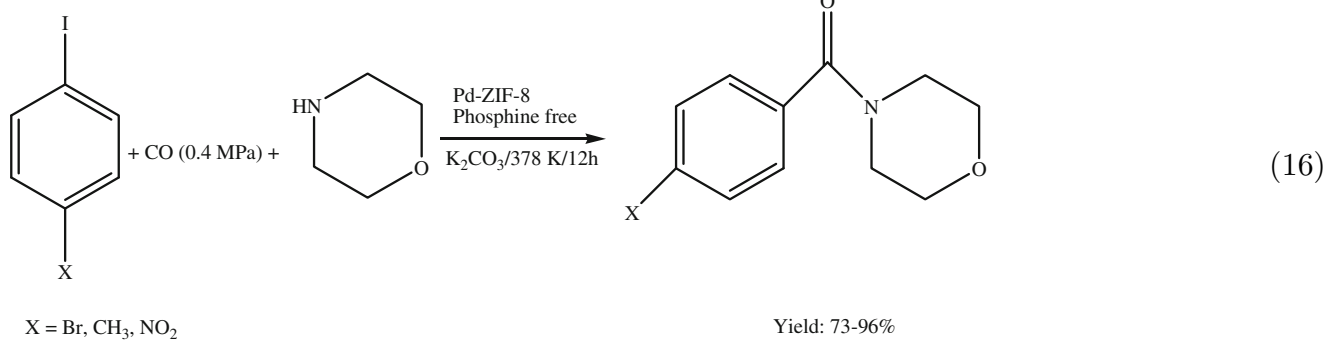
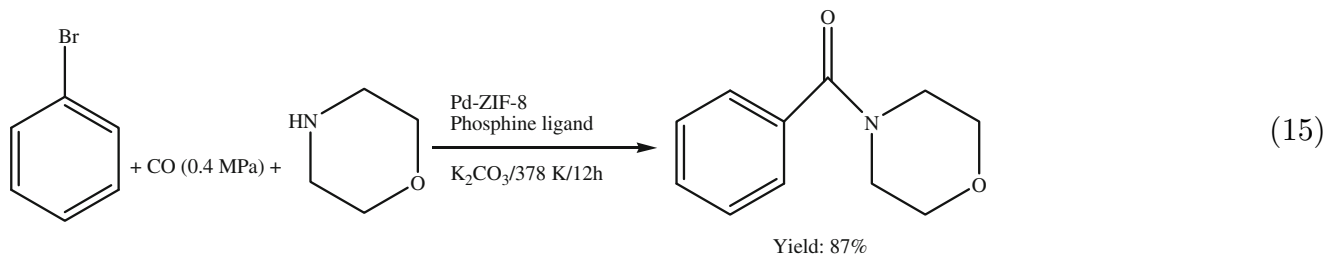
than the pore apertures of ZIF-8 shells (3.4 Å), indicating the molecular-size selectivity of the microporous ZIF-8, where the active sites were located inside the ZIF matrix, whereas Pd on ZIF-8 showed activity in cyclooctene hydrogenation because the Pd nanocrystals on ZIF-8 had formed on the external surface of ZIF-8.

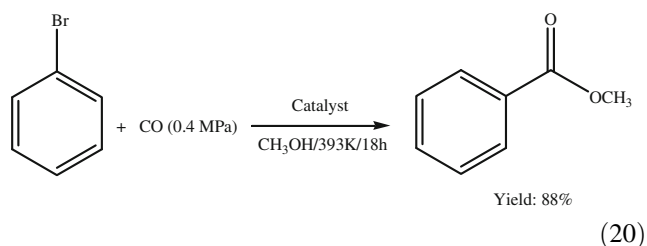
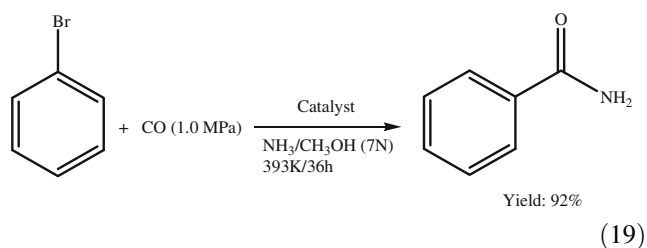
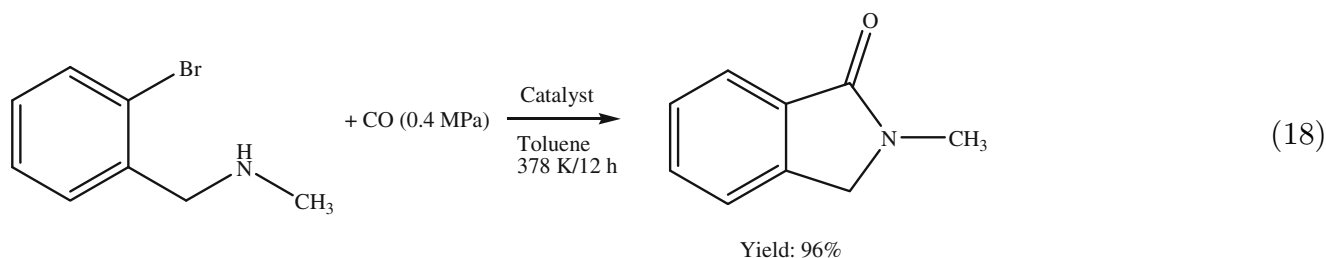
5.8 Reduction of 4-Nitrophenol



Bimetallic Au-Ag core-shell onto ZIF-8 and Au nanoparticles onto ZIF-8 were applied to the catalytic reduction of 4-nitrophenol by NaBH₄ in the aqueous phase as in (14), and 4-nitrophenol were converted to the product in good yield within a short reaction time (10-28 min), as measured by UV-visible spectroscopy [91, 92]. The catalytic performance of the bimetallic Au-Ag core-shell nanoparticles was superior to the alloy or monometallic nanoparticles, due to the strong bimetallic synergistic effect of the core-shell structure of Au-Ag nanoparticles [92].

5.9 Aminocarbonylation of Bromoarene and Iodoarene

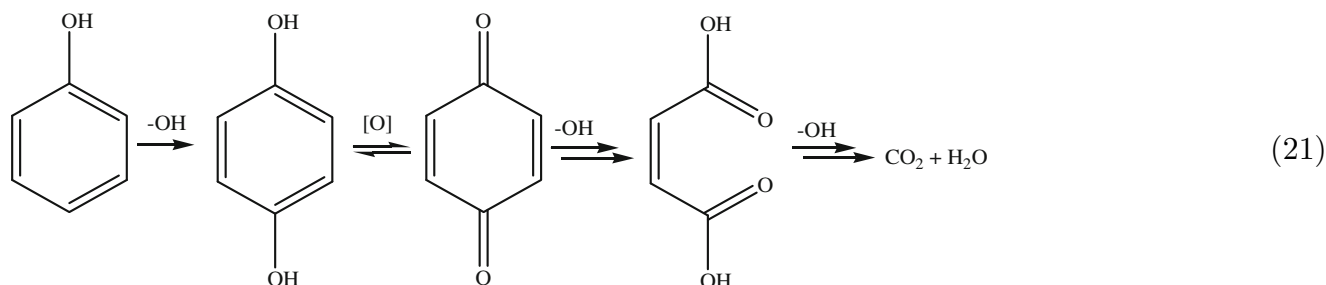


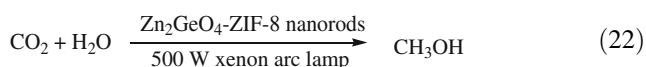


The Pd nanoparticles supported on ZIF-8 (1 wt% Pd) were found to be an efficient heterogeneous catalyst for the aminocarbonylation of a variety of bromoarenes with the phosphine ligand as in (15) and iodoarenes under phosphine-free conditions in (16) using a base in toluene at 378 K, in which the Pd nanoparticles are located on the external surface of the ZIF-8 [17]. It was suggested that the adsorbed phosphine ligand around Pd nanoparticles may modify the electronic properties to accelerate the oxidative

addition step or promote the reductive elimination step and stabilize Pd nanoparticles to prevent aggregation. The use of insoluble inorganic bases (K_2CO_3 and K_3PO_4) provided higher activity than the soluble organic bases (Hünig base, 1,8-diazabicyclo[5.4.0]undec-7-ene and C_2H_5N). The authors also reported the preparation of several pharmaceutically important chemicals, CX-546 (95 % yield), moclobemide (96 % yield), nikethamide (92 % yield) and procainamide (75 % yield), using this catalytic system. The amide yield in the aminocarbonylation of *p*-bromotoluene and morpholine for the four repeated runs remained relatively constant. The heterogeneity of the Pd-ZIF-8 catalyst in the liquid phase reaction was confirmed by hot filtration experiments, but the leaching of Pd (<4 ppm) was observed in the filtrate solution after recycling. The catalyst was applied to the one-pot aminocarbonylation of aryl bromides and iodides under the phosphine ligand-control reaction to produce bisamide as in (17) in 72 % yield. This catalyst system was also useful for the preparation of cyclic amides, primary amides and esters from the carbonylation of phenyl bromide as in (18)-(20) in high yield (88–96 %).

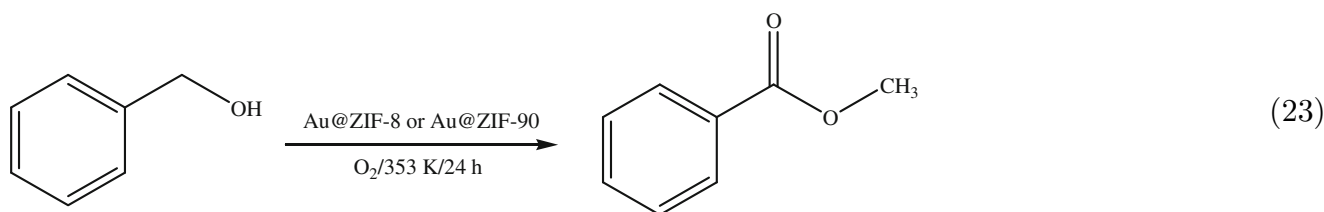
5.10 Photodegradation of Phenol and the Photocatalytic Reduction of CO_2





The Pt-ZIF-8-loaded TiO₂ nanotubes showed higher degradation efficiency (18.6 %) in the photodegradation of phenol in an aqueous solution in (21) under visible light

light absorption by Zn₂GeO₄-ZIF-8 generates methanol in higher yield than Zn₂GeO₄. A loading of Pt on the Zn₂GeO₄-ZIF-8 nanorods as a co-catalyst was required to further improve the level of methanol generation. XRD of the Zn₂GeO₄-ZIF-8 nanorods confirmed that the structure had been retained after photocatalytic light irradiation.

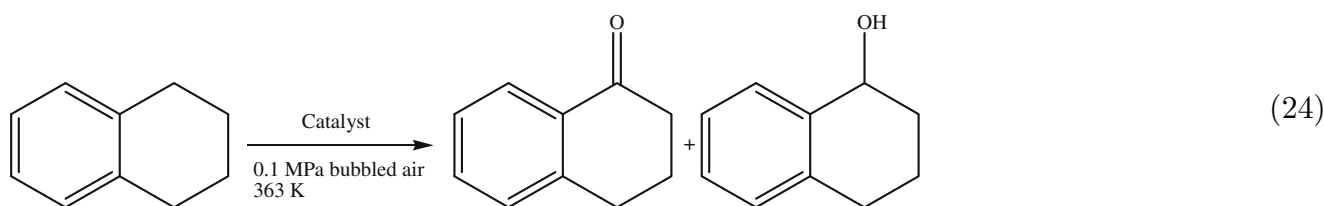


illumination after 2 h than the Pt-TiO₂ nanotubes (~3 %) under similar reaction conditions [87]. The generation of hydroxyl radicals by Pt-ZIF-8-loaded TiO₂ nanotubes in the presence of visible light and the attack of hydroxyl radicals to phenol were proposed to be the reaction pathway for the formation of carbon dioxide and water over a Pt-ZIF-8 loaded TiO₂ nanotube composite with a lower band gap of 2.65 eV. Cu-doped ZIF-67 (Cu-ZIF-67) was applied to the photocatalytic degradation of methyl orange under visible light illumination [56]. Cu-ZIF-67 exhibited higher activity than ZIF-67 due to the presence of Cu⁺ ions in the Cu-ZIF-67 structure. Cu-ZIF-67 showed similar photocatalytic degradation of the number of repeated runs.

The semiconductor-MOF nanocomposite, Zn₂GeO₄-ZIF-8 (ZIF-8 nanoparticles onto Zn₂GeO₄ nanorods), was used as a photocatalyst for the reduction of CO₂ in an aqueous solution as in (22) to form methanol (yield of

5.11 Aerobic Oxidation of Benzyl Alcohol

Esken et al. [14] reported the catalytic activity of Au nanoparticles supported on ZIF-8 and ZIF-90 for the liquid-phase aerobic oxidation of benzyl alcohol to methyl benzoate in methanol using pure oxygen (0.5 MPa) as in (23). The Au nanoparticles supported on ZIF-8 showed higher activity (81.2 % conversion and 98.2 % selectivity to methyl benzoate) than the Au nanoparticles supported on ZIF-90 (12.74 % conversion and 50.55 % selectivity to methyl benzoate) at 353 K after 24 h. The low activity over the Au nanoparticles supported on ZIF-90 catalyst was attributed to the in situ oxidation of the -CHO group of ZIF-90 in the presence of Au nanoparticles to imidazolates-2-methylcarboxylate. The catalysis reaction occurred on the inside of the pores of the ZIF matrices, where the active Au nanoparticles were encapsulated.

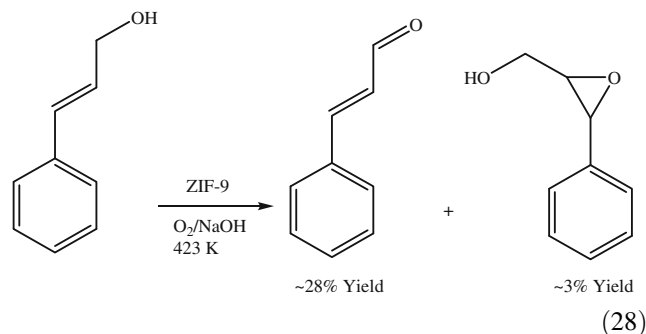


~2.44 μmol/g after 11 h). The catalytic performance of the Zn₂GeO₄-ZIF-8 nanocomposite was superior to that of the bare Zn₂GeO₄ nanorods (methanol yield of ~1.43 μmol/g) [38]. The mechanism proposed was that the dissolved CO₂ in water is adsorbed on ZIF-8 and the

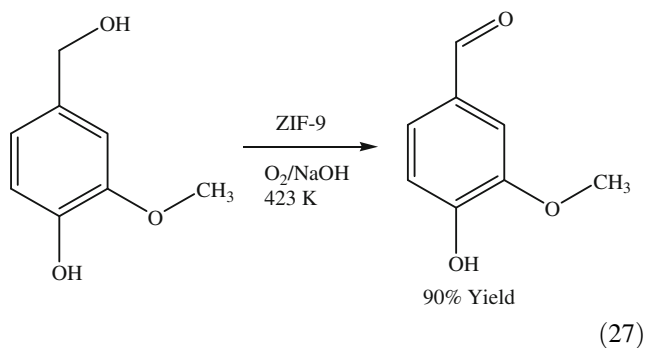
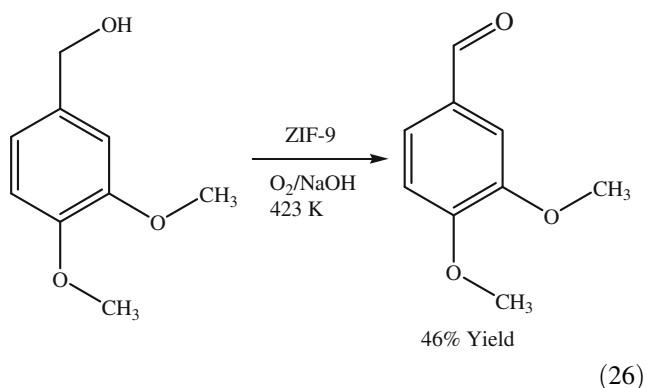
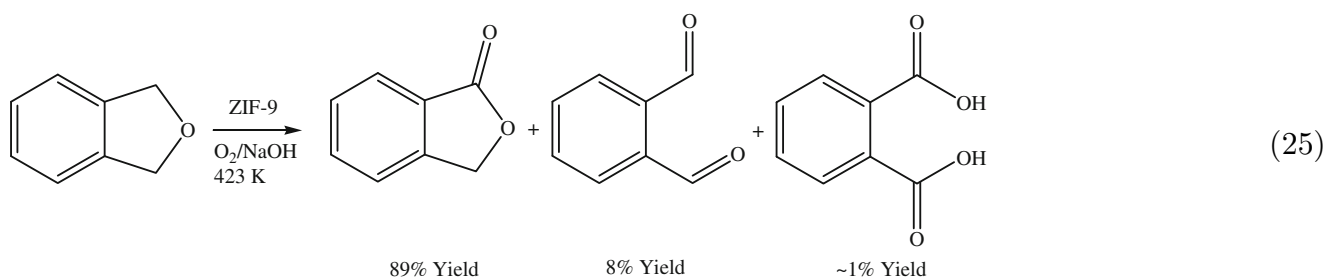
5.12 Aerobic Oxidation of Tetralin

Llabrés i Xamena et al. [12] reported the use of Co(II) in ZIF-9 as a catalytic oxidation site for the liquid-phase oxidation of tetralin using air as the oxidant as in (24).

A tetralin conversion of 23.2 mol% and the product tetralone/tetralol molar ratio of 6.8 were obtained at 363 K after 24 h with a large induction period (~10 h). The conversion over the fresh catalyst decreased only slightly upon recycling, and no Co leaching was observed. The mixture of ZIF-9/Cu-MOF (90/10 wt%) (Cu-MOF, a Cu-containing MOF of composition $[\text{Cu}(2\text{-hydroxypyrimidinolate})_2] \cdot 2.25\text{H}_2\text{O}$) resulted in sharp decrease in the induction period accompanied by the enhancement in tetralin conversion (31 %) and good product selectivity.



5.13 Oxidation of Aromatic Oxygenates



Cobalt-based catalytic systems with molecular oxygen are highly active catalysts for the oxidation of aromatic alcohols and cyclic ethers [99–101], in which cobalt is activated with molecular oxygen to form a radical intermediate for substrate oxidation. ZIF-9 was applied to the oxidation of aromatic oxygenates using molecular oxygen (0.5 MPa) at 423 K, and various aromatic substrates, such as phthalan, veratryl alcohol, vanillyl alcohol, and cinnamyl alcohol, were converted selectively to commercially important aldehydes as in (25)–(28) in good yield [102]. The heterogeneity of the catalyst was confirmed using a hot filtration experiment. The Co content after catalytic reaction was measured by ICP analysis and XRD, UV–Vis spectroscopy. Catalysis occurred on the external surface of ZIF-9.

6 Adsorption

The adsorption of gases of primary industrial significance over the MOFs can involve the following processes: (1) CO_2/N_2 or CO_2/CH_4 separation for carbon capture and sequestration (CCS) or natural gas or biogas purification, (2) natural gas (CH_4) and H_2 storage as an alternative to petroleum-based fuels for automobiles, and (3) alkene/alkane separation in the petrochemical industry. Both the

Table 5 Adsorption studies carried out over ZIFs

ZIF	Guest species	Comments	Ref.
ZIF-8	H ₂ /CH ₄	Isotherms over 30-300 K up to 65 bar (volumetric) Maximal H ₂ and CH ₄ capacities limited to 4.4 and 22.4 wt % Functionalization essential for energy storage	[109]
ZIF-8	CH ₄	Neutron powder diffraction study CH ₄ primarily adsorbed on the organic linkers	[110]
ZIF-8	H ₂ O	Water physisorption properties: comparison with other MOFs	[111]
ZIF-8	N ₂ /n-Hexane	The effects of pressure, temperature, feed conditions, and n-alkane (C5 – C7) components on the separation performances of ZIF-8 membranes for N ₂ /alkane(s)	[112]
ZIF-8	n-Hexane, 2-methylpentane, 2,2-dimethylbutane, 2,3-dimethylbutane	Combined experimental/modeling approach ZIF-8 is selective for n-hexane and excludes the bulky 2,2-dimethylbutane	[113]
ZIF-8	Propane/Propene	Synthesis of 2 ZIF with sodalite (sod) framework structures using 2-Cl- and 2-Br-imidazole for olefin/paraffin separation: effect of pore size	[114]
ZIF-8	Ethene/Ethane	ZIF-8 membrane Separation of ethene and ethane at RT for 1 and 6 bar	[115]
ZIF-8	Xylene isomers (ortho, meta, para)	Separation of xylene isomers in the gas and liquid phase Gas phase separation is better	[116]
ZIF-8	EtOH/H ₂ O	The EtOH/water separation capability of ZIF-8 with different size	[117]
ZIF-8 ZIF-90	MeOH/EtOH	Combined experimental/modeling approach ZIF-90 showed significantly higher alcohol uptake Diffusion selectivity of methanol over ethanol is significantly higher in ZIF-8	[118]
ZIF-8	MeOH, EtOH,	Applying ZIFs for bio-alcohols separation	[119]
ZIF-71	1-PrOH, 2-PrOH,	ZIF-8 and ZIF-71 for the extraction of butyl/propyl alcohols from H ₂ O	
ZIF-90	1-butanol, H ₂ O		
ZIF-7	EtOH, n-PrOH,	Experimental/simulation study for bio-alcohol separation	[120]
ZIF-8	n-butanol, n-pentanol	ZIF-8 showed exceptional adsorption selectivity and capacity toward iso-butanol molecules	
ZIF-8	MeOH, EtOH, n-PrOH, n-butanol	Simulation for normal alcohols adsorption The interaction between alcohol and ZIF-8 is enhanced as the chain length of alcohol increases	[121]
ZIF-8	Pigment	Pigment entrapping inside ZIF-8	[122]
ZIF-8	Caffeine	Introduction of caffeine to ZIF-8 by two different methods: in situ and ex situ encapsulation	[123]
ZIF-8	H ₂ -PA, DEP	High H ₂ -PA removal from aqueous solution by ZIF-8	[124]

MeOH methanol, *EtOH* ethanol, *PrOH* propanol, *H₂-PA* phthalic acid, *DEP* diethyl phthalate

powder and membrane forms have been considered for these applications. For ZIFs, CO₂ adsorption is currently the most widely investigated topic, and brief statements will be made here in relation to their ligand functionalization.

A comparison of the performance of zeolite 13X and other microporous materials with ZIF-8 for CO₂ adsorption at low pressures indicated that ZIF-8 exhibited significantly less CO₂ uptake and moderate selectivity with a low heat of adsorption compared to 13X [103, 104], despite its strong hydrophobicity, water stability, and total reversibility in adsorption.

Subsequently, efforts have been made to improve the CO₂ capture performance of ZIF-8 using linker functionalization. The CO₂ uptake at 0.1 MPa 25 C varied in the

following sequence: ZIF-78 (–NO₂) > ZIF-82, -81, -69 (–CN, –Br, –Cl) > ZIF-68,-79 (–C₆H₆, –CH₃) > ZIF-70 (–H) > BPL carbon, which suggests the greater attraction between polar functional groups in ZIFs and CO₂ [5]. The textural properties of the ZIFs were not important, and ZIF-78 captured approximately 3 times the CO₂ captured by BPL carbon at 0.1 MPa. An experimental and computational study of ligand functionalization in the *sod* ZIF structures of ZIF-8, ZIF-90 and ZIF-Cl also indicated that modifying the linker (dipole moment) can lead to a 5–7 fold improvement in CO₂ selectivity for CO₂/CH₄, CO₂/N₂, and CO₂/CO mixtures [105]. Recently, Thompson et al. [106] reported improved performance of two types of mixed linker ZIF systems over ZIF-8 for CO₂ selectivity in

CO₂/CH₄ separation: ZIF-8 comprised of 2-methylimidazole and 2-aminobenzimidazole linkers, and ZIF-8-90 comprised of a 50:50 mol ratio of HMeIM (for ZIF-8) and carboxaldehyde-2-imidazole (for ZIF-90) followed by post-synthesis functionalization with ethylenediamine.

ZIF-95 and ZIF-100 are thermally stable up to 773 K, and their huge cavities (2.4 and 3.6 nm, respectively) combined with highly constricted windows (3.65 and 3.35 Å, respectively) as well as the strong quadrupolar interaction of CO₂ with N atoms in the imidazolate linkers highlight the excellent performance in CO₂ capture with high selectivity (CO₂/N₂ = 18 and 25, respectively) and high CO₂ capture capacity at 0.1 MPa [3]. One liter of ZIF-100 can store 28.2 L of CO₂ at 273 K and 15.9 L at 298 K under ambient pressures. Both ZIFs also exhibited complete reversibility in adsorption. Some MOFs had a higher CO₂ capture capacity, but did not exhibit the selectivity achieved by the ZIFs. Zeolite-like metal organic framework (ZMOF) materials prepared using 4,5-imidazoledicarboxylic acid as a bridging linker and indium (III) as a metal source in *rho* and *sod* topologies were also tested experimentally for CO₂ adsorption. The results revealed significantly enhanced CO₂ adsorption and higher selectivity than those by ZIF-8 [107]. Partially alkali-ion exchanged *sod* ZMOFs resulted in further improvement in the CO₂ capture performance. ZIF-11 was predicted to satisfy the industrial feasibility target for H₂/CO₂ and H₂/N₂ separations for pre-combustion carbon capture, and simulation studies revealed ZIF-8,-90 and -77 to be candidate materials for natural gas purification (CO₂/CH₄) [108]. Table 5 summarizes the experimental studies carried out for other adsorption applications [109–124].

7 Concluding Remarks

A large number of ZIF materials have been synthesized solvothermally in organic solvents with some also synthesized in water. On the other hand, the number of ZIF structures being tested in catalytic/adsorption applications is limited due to the difficulties in reproducible ZIF synthesis employing mixed ligands, as well as the high ligand cost. The window size of the most ZIFs are limited to ca. 3.5 Å, which needs to be increased for broader applications in catalysis/adsorption.

A synthesis scale-up study is necessary. Despite some success in the high-throughput syntheses of ZIFs, a synthesis scale up even to gram quantities is a challenge, particularly for mixed hetero-linker systems. A synthesis procedure for multi-gram scales also needs to be established using environmentally benign techniques.

ZIFs have high thermal and chemical stability, which makes them good candidate materials for adsorption/

catalysis in an industrial perspective. Although ZIFs can be synthesized directly with functionalized organic linkers, the post-synthesis modification of ZIF can offer new materials with desirable properties for the synthesis of fine chemicals, such as for a tandem reaction that displays high atomic utilization efficiency and does not involve workup and isolation of many intermediates. The improved CO₂ capture performance by organic-functionalized ZIFs is also well-established, which had already shown the efficient separation of CO₂ from a range of gas mixtures, such as in CO₂/CH₄, CO₂/CO, CO₂/N₂.

The Lewis acid Zn²⁺ and nitrogen base sites in ZIF-8 are active sites for adsorption and catalysis, and noble metals deposited on ZIFs also frequently show promising catalytic activities. On the other hand, in some cases, Zn or noble metals can be leached during the liquid phase catalytic reactions caused by moderately high reaction temperatures or solvents. The stability of the system needs to be monitored closely.

ZIF-8 crystals can grow on magnetic microspheres, semiconductors or polymer/inorganic membranes. The immobilization of noble metal nanoparticles on ZIF materials can produce a wide range nanoparticle-supported ZIFs. The number of such composite or supported materials, which can be applied to catalysis for the preparation of drug molecules and pharmaceutical chemicals or as photocatalysts, is expected to grow in the near future.

Acknowledgments This study was supported by a National Research Foundation of Korea (NRF) Grant funded by the Korean Government (MEST) (No. 2013005862).

References

1. Park KS, Ni Z, Côté AP, Choi JY, Huang R, Uribe-Romo FJ, Chae HK, O’Keeffe M, Yaghi OM (2006) *PNAS* 103:10186
2. Banerjee R, Phan A, Wang B, Knobler C, Furukawa H, O’Keeffe M, Yaghi OM (2008) *Science* 319:939
3. Wang B, Côté AP, Furukawa H, O’Keeffe M, Yaghi OM (2008) *Nature* 453:207
4. Phan A, Doonan CJ, Uribe-Romo FJ, Knobler CB, O’Keeffe M, Yaghi OM (2010) *Acc Chem Res* 43:58
5. Banerjee R, Furukawa H, Britt D, Knobler C, O’Keeffe M, Yaghi OM (2009) *J Am Chem Soc* 131:3875
6. Hayashi H, Côté AP, Furukawa H, O’Keeffe M, Yaghi OM (2007) *Nat Mater* 6:501
7. Bux H, Liang F, Li Y, Cravillon J, Wiebcke M, Caro J (2009) *J Am Chem Soc* 131:16000
8. Li YS, Liang FY, Bux H, Feldhoff A, Yang WS, Caro J (2010) *Angew Chem Int Ed* 49:548
9. Fairen-Jimenez D, Moggach SA, Wharmby MT, Wright PA, Parsons S, Düren T (2011) *J Am Chem Soc* 133:8900
10. Huang XC, Lin YY, Zhang JP, Chen XM (2006) *Angew Chem Int Ed* 45:1557
11. Chen R, Yao J, Gu Q, Smeets S, Baerlocher C, Gu H, Zhu D, Morris W, Yaghi OM, Wang H (2013) *Chem Commun* 49:9500
12. Llabrés i Xamena FX, Casanova O, Taillefer RG, Garcia H, Corma A (2008) *J Catal* 255:220

13. Chizallet C, Lazare S, Bazer-Bachi D, Bonnier F, Lecocq V, Soyer E, Quoineaud AA, Bats N (2010) *J Am Chem Soc* 132:12365
14. Esken D, Turner S, Lebedev OI, Tendeloo GV, Fischer RA (2010) *Chem Mater* 22:6393
15. Miralda CM, Macias EE, Zhu M, Ratnasamy P, Carreon MA (2012) *ACS Catal* 2:180
16. Cho HY, Kim J, Kim SN, Ahn WS (2013) *Micropor Mesopor Mater* 169:180
17. Dang TT, Zhu Y, Ngiam JSY, Ghosh SC, Chen A, Seayad AM (2013) *ACS Catal* 3:1406
18. Férey G (2008) *Chem Soc Rev* 37:191
19. Wang Z, Cohen SM (2009) *Chem Soc Rev* 38:1315
20. Czaja AU, Trukhan N, Müller U (2009) *Chem Soc Rev* 38:1284
21. Lee JY, Farha OK, Roberts J, Scheidt KA, Nguyen ST, Hupp JT (2009) *Chem S Rev* 38:1450
22. Fang QR, Makal TA, Young MD, Zhou HC (2010) *Comments Inorg Chem* 31:165
23. Corma A, García H, Xamena FXLI (2010) *Chem Rev* 110:4606
24. Kim M, Cohen SM (2012) *CrystEngComm* 14:4096
25. Stock N, Biswas S (2012) *Chem Rev* 112:933
26. Song L, Zhang J, Sun L, Xu F, Li F, Zhang H, Si X, Jiao C, Li Z, Liu S, Liu Y, Zhou H, Sun D, Du Y, Cao Z, Gabelica Z (2012) *Energy Environ Sci* 5:7508
27. Furukawa H, Cordova KE, O'Keeffe M, Yaghi OM (2013) *Science* 341:1230444
28. Kim J, Cho HY, Ahn WS (2012) *Catal Surv Asia* 16:106
29. Yao J, Wang H (2014) *Chem Soc Rev*. doi:10.1039/c3cs60480b
30. Nune SK, Thallapally PK, Dohnalkova A, Wang C, Liu J, Exarhos GJ (2010) *Chem Commun* 46:4878
31. Pan Y, Liu Y, Zeng G, Zhao L, Lai Z (2011) *Chem Commun* 47:2071
32. Thompson JA, Chapman KW, Koros WJ, Jones CW, Nair S (2012) *Micropor Mesopor Mater* 158:292
33. Fu YY, Yang CX, Yan XP (2013) *Chem Eur J* 19:13484
34. Yang Y, Ge L, Rudolph V, Zhu Z (2014) *Dalton Trans* 43:7028
35. Sue YC, Wu JW, Chung SE, Kang CH, Tung KL, Wu KCW, Shieh FK (2014) *ACS Appl Mater Interfaces* 6:5192
36. Zhang T, Zhang X, Yan X, Kong L, Zhang G, Liu H, Qiu J, Yeung KL (2013) *Chem Eng J* 228:398
37. Jin R, Bian Z, Li J, Ding M, Gao L (2013) *Dalton Trans* 42:3936
38. Liu Q, Low ZX, Li L, Razmjou A, Wang K, Yao J, Wang H (2013) *J Mater Chem A* 1:11563
39. Park JH, Park SH, Jung SH (2009) *J Korean Chem Soc* 53:553
40. Yang L, Lu H (2012) *Chin J Chem* 30:1040
41. Bao Q, Lou Y, Xing T, Chen J (2013) *Inorg Chem Commun* 37:170
42. Seoane B, Zamaro JM, Tellez C, Coronas J (2012) *CrystEngComm* 14:3103
43. Beldon PJ, Fábian L, Stein RS, Thirumurugan A, Cheetham AK, Friščić T (2010) *Angew Chem Int Ed* 49:9640
44. Friščić T, Halasz I, Beldon PJ, Belenguer AM, Adams F, Kimber SAJ, Honkimäki V, Dinnebier RE (2013) *Nature Chem* 5:66
45. Tanaka S, Kida K, Nagaoka T, Ota T, Miyake Y (2013) *Chem Commun* 49:7884
46. Li R, Ren X, Ma H, Feng X, Lin Z, Li X, Hu C, Wang B (2014) *J Mater Chem A* 2:5724
47. Li R, Ren X, Zhao J, Feng X, Jiang X, Fan X, Lin Z, Li X, Hu C, Wang B (2014) *J Mater Chem A* 2:2168
48. Shi Q, Chen Z, Song Z, Li J, Dong J (2011) *Angew Chem Int Ed* 50:672
49. Lin JB, Lin RB, Cheng XN, Zhang JP, Chen XM (2011) *Chem Commun* 47:9185
50. Lanchas M, Vallejo-Sánchez D, Beobide G, Castillo O (2012) *Chem Commun* 48:9930
51. Faustini M, Kim J, Jeong GY, Kim JY, Moon HR, Ahn WS, Kim DP (2013) *J Am Chem Soc* 135:14619
52. Yamamoto D, Maki T, Watanabe S, Tanaka H, Miyahara MT, Mae K (2013) *Chem Eng J* 227:145
53. Joaristi AM, Juan-Alcañiz J, Serra-Crespo P, Kapteijn F, Gascon J (2012) *Cryst Growth Des* 12:3489
54. Lee YR, Kim J, Ahn WS (2013) *Korean J Chem Eng* 30:1667
55. Nguyen LTL, Le KKA, Truong HX, Phan NTS (2012) *Catal Sci Technol* 2:521
56. Yang H, He XW, Wang F, Kang Y, Zhang J (2012) *J Mater Chem* 22:21849
57. Lively RP, Dose ME, Thompson JA, McCool BA, Chance RR, Koros WJ (2011) *Chem Commun* 47:8667
58. Morris W, Leung B, Furukawa H, Yaghi OK, He N, Hayashi H, Houndonogbo Y, Asta M, Laird BB, Yaghi OM (2010) *J Am Chem Soc* 132:11006
59. Liu S, Liu G, Zhao X, Jin W (2013) *J Membr Sci* 446:181
60. Dong X, Lin YS (2013) *Chem Commun* 49:1196
61. Pérez-Pellitero J, Amrouche H, Siperstein FR, Pirngruber G, Nieto-Draghi C, Chaplais G, Simon-Masseron A, Bazer-Bachi D, Peralta D, Bats N (2010) *Chem Eur J* 16:1560
62. Ban Y, Li Y, Liu X, Peng Y, Yang W (2013) *Micropor Mesopor Mater* 173:29
63. Dong X, Huang K, Liu S, Ren R, Jin W, Lin YS (2012) *J Mater Chem* 22:19222
64. Fan L, Xue M, Kang Z, Wei G, Huang L, Shang J, Zhang D, Qiu S (2014) *Micropor Mesopor Mater* 192:29
65. Yu LQ, Yan XP (2013) *Chem Commun* 49:2142
66. Morris W, Doonan CJ, Furukawa H, Banerjee R, Yaghi OM (2008) *J Am Chem Soc* 130:12626
67. Yu LQ, Yang CX, Yan XP (2014) *J Chromatogr A* 1334:1
68. Yang T, Chung TS (2013) *J Mater Chem A* 1:6081
69. Shieh FK, Wang SC, Leo SY, Wu KCW (2013) *Chem Eur J* 19:11139
70. Xu YP, Tian ZJ, Wang SJ, Hu Y, Wang L, Wang BC, Ma YC, Hou L, Yu JY, Lin LW (2006) *Angew Chem Int Ed* 45:3965
71. Choi JS, Son WJ, Kim J, Ahn WS (2008) *Micropor Mesopor Mater* 116:727
72. Gedanken A (2004) *Ultrason Sonochem* 11:47
73. Štrukil V, Fábian L, Reid DG, Duer MJ, Jackson GJ, Eckert-Maksić M, Friščić T (2010) *Chem Commun* 46:9191
74. Friščić T, Halasz I, Štrukil V, Eckert-Maksić M, Dinnebier RE (2012) *Croat Chem Acta* 85:367
75. Garay AL, Pichon A, James SL (2007) *Chem Soc Rev* 36:846
76. Friščić T, Fábian L (2009) *CrystEngComm* 11:743
77. Kim J, Lee YR, Ahn WS (2013) *Chem Commun* 49:7647
78. Matsukata M, Ogura M, Osaki T, Rao PRHP, Nomura M, Kikuchi E (1999) *Top Catal* 9:77
79. Ahmed I, Jeon J, Khan NA, Jung SH (2012) *Cryst Growth Des* 12:5878
80. Abou-Hassan A, Sandre O, Cabuil V (2010) *Angew Chem Int Ed* 49:6268
81. Ameloot R, Vermoortele F, Vanhove W, Roeffaers MJB, Sels BF, Vos DED (2011) *Nature Chem* 3:382
82. Huang A, Dou W, Caro J (2010) *J Am Chem Soc* 132:15562
83. Huang A, Wang N, Kong C, Caro J (2012) *Angew Chem Int Ed* 51:10551
84. Karagiari O, Lalonde MB, Bury W, Sarjeant AA, Farha OK, Hupp JT (2012) *J Am Chem Soc* 134:18790
85. Pan Y, Ma D, Liu H, Wu H, He D, Li Y (2012) *J Mater Chem* 22:10834
86. Wang P, Zhao J, Li X, Yang Y, Yang Q, Li C (2013) *Chem Commun* 49:3330
87. Isimjan TT, Kazemian H, Rohani S, Ray AK (2010) *J Mater Chem* 20:10241

88. Lu G, Li S, Guo Z, Farha OK, Hauser BG, Qi X, Wang Y, Wang X, Han S, Liu X, DuChene JS, Zhang H, Zhang Q, Chen X, Ma J, Loo SCJ, Wei WD, Yang Y, Hupp JT, Huo F (2012) *Nature Chem* 4:310
89. Zahmakiran M (2012) *Dalton Trans* 41:12690
90. Liu M, Fan B, Shi X, Li R (2013) *Catal Commun* 42:20
91. Li Z, Zeng HC (2013) *Chem Mater* 25:1761
92. Jiang HL, Akita T, Ishida T, Haruta M, Xu Q (2011) *J Am Chem Soc* 133:1304
93. Kuo CH, Tang Y, Chou LY, Sneed BT, Brodsky CN, Zhao Z, Tsung CK (2012) *J Am Chem Soc* 134:14345
94. Tran UPN, Le KKA, Phan NTS (2011) *ACS Catal* 1:120
95. Kim J, Kim SN, Jang HG, Seo G, Ahn WS (2013) *Appl Catal A Gen* 453:175
96. Zhu M, Srinivas D, Bhogeswararao S, Ratnasamy P, Carreon MA (2013) *Catal Commun* 32:36
97. Nguyen LTL, Le KKA, Phan NTS (2012) *Chin J Catal* 33:688
98. Wee LH, Lescouet T, Ethiraj J, Bonino F, Vidruk R, Garrier E, Packet D, Bordiga S, Farrusseng D, Herskowitz M, Martens JA (2013) *ChemCatChem* 5:3562
99. Zakzeski J, Jongerius AL, Weckhuysen BM (2010) *Green Chem* 12:1225
100. Zakzeski J, Bruijninx PCA, Weckhuysen BM (2011) *Green Chem* 13:671
101. Li P, Alper H (1992) *J Mol Catal* 72:143
102. Zakzeski J, Dębczak A, Bruijninx PCA, Weckhuysen BM (2011) *Appl Catal A Gen* 394:79
103. McEwen J, Hayman JD, Yazaydin AO (2013) *Chem Phys* 412:72
104. Garcés SI, Villarroel-Rocha J, Sapag K, Korili SA, Gil A (2013) *Ind Eng Chem Res* 52:6785
105. Amrouche H, Aguado S, Pérez-Pellitero J, Chizallet C, Siperstein F, Farrusseng D, Bats N, Nieto-Draghi C (2011) *J Phys Chem C* 115:16425
106. Thompson JA, Brunelli NA, Lively RP, Johnson JR, Jones CW, Nair S (2013) *J Phys Chem C* 117:8198
107. Chen C, Kim J, Yang DA, Ahn WS (2011) *Chem Eng J* 168:1134
108. Thornton AW, Dubbeldam D, Liu MS, Ladewig BP, Hill AJ, Hill MR (2012) *Energy Environ Sci* 5:7637
109. Zhou W, Wu H, Hartman MR, Yildirim T (2007) *J Phys Chem C* 111:16131
110. Wu H, Zhou W, Yildirim T (2009) *J Phys Chem C* 113:3029
111. Gee JA, Chung J, Nair S, Sholl DS (2013) *J Phys Chem C* 117:3169
112. Li J, Zhong J, Huang W, Xu R, Zhang Q, Shao H, Gu X (2014) *Ind Eng Chem Res* 53:3662
113. Küsgens P, Rose M, Senkovska I, Fröde H, Henschel A, Siegle S, Kaskel S (2009) *Micropor Mesopor Mater* 120:325
114. Zhang K, Lively RP, Dose ME, Brown AJ, Zhang C, Chung J, Nair S, Koros WJ, Chance RR (2013) *Chem Commun* 49:3245
115. Liu XL, Li YS, Zhu GQ, Ban YJ, Xu LY, Yang WS (2011) *Angew Chem Int Ed* 50:10636
116. Jankowska A, Florczak P, Kowalak S (2013) *Micropor Mesopor Mater* 171:78
117. Ferreira AFP, Mittelmeijer-Hazeleger MC, Granato MA, Duarte Martins VF, Rodrigues AE, Rothenberg G (2013) *Phys Chem Chem Phys* 15:8795
118. Zhang K, Zhang L, Jiang J (2013) *J Phys Chem C* 117:25628
119. Bux H, Chmelik C, Krishna R, Caro J (2011) *J Membr Sci* 369:284
120. Zhang K, Lively RP, Zhang C, Koros WJ, Chance RR (2013) *J Phys Chem C* 117:7214
121. Peralta D, Chaplais G, Paillaud JL, Simon-Masseron A, Barthelet K, Pirngruber GD (2013) *Micropor Mesopor Mater* 173:1
122. Liédana N, Galve A, Rubio C, Téllez C, Coronas J (2012) *ACS Appl Mater Interfaces* 4:5016
123. Li K, Olson DH, Seidel J, Emge TJ, Gong H, Zeng H, Li J (2009) *J Am Chem Soc* 1231:10368
124. Khan NA, Jung BK, Hasan Z, Jhung SH (2014) *J Hazard Mater*. doi:10.1016/j.jhazmat.2014.03.047